UNIVERSITY OF GENOVA

POLYTECHNIC SCHOOL

DIME

Department of Mechanical, Energy, Management and Transportation Engineering

MASTER THESIS
IN
MECHANICAL ENGINEERING

Study of Gas Permeability across Polymers at Low Temperature

Supervisor:

Chiar.mo Prof. Ing. Carla Gambaro

CERN Supervisor:

Dr. Torsten Koettig

Candidate:

Giulia Cudia

December 2019

UNIVERSITY OF GENOVA

POLYTECHNIC SCHOOL

DIME

Department of Mechanical, Energy, Management and Transportation Engineering

MASTER OF SCIENCE THESIS
IN
MECHANICAL ENGINEERING

Study of Gas Permeability across Polymers at Low Temperature

Supervisor:

Chiar.mo Prof. Ing. Carla Gambaro

CERN Supervisor:

Dr. Torsten Koettig

Candidate:

Giulia Cudia

December 2019

Studio della Permeabilità di Gas in Materiali Polimerici a Basse Temperature

Sommario

Lo studio della permeabilità dei gas attraverso materiali polimerici è argomento di interesse in molti campi della scienza e della tecnologia: ad esempio, le membrane polimeriche sono largamente utilizzate sia come barriere contro i gas atmosferici, sia per separare i differenti gas in campo medico ed industriale; i polimeri caratterizzati da una maggiore proprietà di barriera vengono utilizzati per l'imballaggio di bibite analcoliche gassate, dove impediscono la permeazione del diossido di carbonio, dell'ossigeno e dell'acqua; possono inoltre essere usati per contenere grassi e olii, i quali devono essere preservati dall'azione ossidante dell'ossigeno.

Il presente lavoro di tesi è incentrato sullo studio dei meccanismi di diffusione e permeazione di gas attraverso membrane polimeriche a basse temperature, per una loro possibile applicazione in sistemi da ultra-alto vuoto (in inglese Ultra High Vacuum, UHV) e in alcuni esperimenti criogenici del CERN. Tale studio è stato svolto con il Gruppo di Criogenia, su commissione del gruppo responsabile dell'esperimento COMPASS (Common Muon and Proton Apparatus for Structure and Spectroscopy®). Tale esperimento presenta un bersaglio costituito da un tubo in Kapton contenente idrogeno liquido, chiuso alle estremità da due tappi in Mylar. La stessa natura dell'esperimento dunque richiede che la diffusione dell'elio e dell'idrogeno attraverso i polimeri di cui sono costituite le pareti del bersaglio sia studiata, a bassa temperatura, per poter separare in modo adeguato il gas contenuto dalle pareti polimeriche dall'ambiente in UHV del fascio di particelle in ingresso.
Le misure sono state condotte in un sistema di permeazione a bassa temperatura, presente nel Laboratorio di Criogenia del CERN, all'interno del quale il materiale polimerico è stato sottoposto a permeazione da parte di alcuni gas di interesse, in particolare Idrogeno ed Elio. Al fine di migliorare le prestazioni del campione in termini di permeabilità alle basse temperature, si è proceduto con una soluzione innovativa che consiste nel diffondere un gas nobile pesante, krypton in questo caso, attraverso il campione a temperatura ambiente; dopo che il krypton è permeato all'interno del campione, si è proceduto con la pulizia dell'impianto, con il raffreddamento alla temperatura di lavoro e con l'iniezione dei gas leggeri di interesse. In questo modo, l'elio e l'idrogeno dovrebbero avere a disposizione meno percorsi liberi attraverso il reticolo del campione, migliorandone la resistenza alla permeabilità.

Lo scopo di questo lavoro è quello di trovare il miglior polimero tra i candidati, che, per composizione e modello strutturale, meglio si presta alla costruzione del nuovo bersaglio di COMPASS, attraverso lo studio della dipendenza dalla temperatura della permeazione e diffusione di idrogeno ed elio attraverso il polimero di interesse.

Study of Gas Permeability across Polymers at Low Temperature

Abstract

The study of permeability of gases through polymeric materials is a topic of interest in many fields of science and technology: for example, polymeric membranes are largely used both as barriers against atmospheric gases and to separate different gases in medical and industrial fields; polymers with high barrier properties are used for packaging of carbonated soft drinks, where they prevent the permeation of carbon dioxide, oxygen and water; they can also be used to contain greases and oils, which have to be preserved from contact with oxygen.

This work focuses on the study of the mechanisms of diffusion and permeation of gases through polymeric membranes at low temperatures, in order to understand if they can be used for Ultra High Vacuum (UHV) applications and for some cryogenic CERN experiments.
This study has been performed in the Cryogenics Group, under commission of the group leading the COMPASS experiment (Common Muon and Proton Apparatus for Structure and Spectroscopy®), which has a target made of liquid hydrogen enclosed inside a Kapton tube with two end-caps in Mylar. By the design concept, the experiment requires the diffusion of the hydrogen and helium through these polymers to be studied at low temperature, to properly separate the target gas from the UHV environment of the particle beam.

Measurements have been performed in a permeating low temperature set-up, present in the CERN Cryogenics Laboratory; the sample has been tested and two gases, hydrogen and helium, have been used as permeants.

To improve the performance of the sample at low temperature an innovative solution has been tested, consisting of diffusing a heavy noble gas, i.e. krypton, through the sample, cooling it down and purging the system before injecting the light gases of interest; in this way, the helium or hydrogen should have a reduced amount of path-ways through the sample, reducing its permeability.

The aim of this work is to find the best polymer sample by composition and structure, among the tested candidates, to be employed for the new target of COMPASS, and to establish the temperature dependance of the permeation and diffusion of hydrogen and helium through its constituent material.

Acknowledgments

I would like to thank my CERN supervisor, Torsten Koettig, for giving me the opportunity to work in this stimulating place, for helping me with his advices and first of all for giving me the feeling to be part of a family also far from home.

I would thank my teacher, Carla Gambaro, for giving me a lot of support in this year, for leading me in difficult decisions and for giving me the free choice of the topic of the thesis.

I thank my colleague and friend Dorothea, for helping me when I needed and for taking care of me in this year at work, and my colleague Antonio, for his technical support with the permeation system.

I thank my sister Marta and my parents, Ignazio e Patrizia, for helping me in every decisions, for being present in all the difficult moments and for leading me in life and work.

I thank my uncles, Nello and Venera, for being present in every important moments of my life and for being since always as my second parents.

I would thank my two best friends, Elisa and Valeria, which I met in two different moments of my life but that are at the same way essential for me in every situation of crisis or joy.

I thank my dear friends of VOLTEggiando for the five years that we spent together, for all the coffee breaks and soirees; these years of university will remain one of my best memories because of you.

I thank my sweet friends Camilla, Chiara, Maddalena and Stella for all the beautiful holidays spent together in these years of university and for those that will come, for your support for the exams, for the laughs and jokes that we enjoyed together.

I would like to thank Eleonora, for being present in every important moment of my growth and university path.

Most of all, I would like to thank Giulia, Raffaello and Francesca: they helped me from the beginning of this experience at CERN, they pushed me to be part of it and they done everything to make me feel as at home. Without them, this experience would not have been possible.

To all of you, thank you.

Riassunto del lavoro di tesi in italiano

L'Organizzazione Europea per la Ricerca Nucleare (CERN) è un centro di ricerca internazionale situato al confine Franco-Svizzero: fu istituito nel 1952 e vanta il complesso di acceleratori di particelle piú grande al mondo. La sua creazione nasce dall'idea di un ristretto numero di scienziati visionari dell'Europa e del Nord America i quali, vedendo la continua fuga di cervelli nel dopo guerra, decisero di unire le forze e creare un centro di ricerca comune. Il complesso degli acceleratori prevede che ogni macchina aumenti in sequenza l'energia di un fascio di particelle prima di iniettarlo in quella successiva. Il fascio nasce da una bottiglia di idrogeno: un campo elettrico scinde gli atomi di idrogeno in elettroni, che vengono scartati, e in protoni che daranno origine al fascio. Il primo acceleratore della catena è Linac 2, segue il Proton Synchrotron Booster (PSB), il Proton Syncrotron (PS), il Super Proton Syncrotron (SPS) ed infine il Large Hadron Collider (LHC), dove il fascio viene diviso in due parti che lo percorrono, rispettivamente, una in senso orario e l'altra in senso antiorario. Nell'LHC i due fasci raggiungono il loro apice di energia, pari a 6.5 TeV per fascio e a 13 TeV nel centro di massa: questo permette di ricreare, durante le collisioni, condizioni simili a quelle teorizzate per i primi nanosecondi successivi al Big Bang. Le collisioni avvengono in quattro punti dell'LHC, in corrispondenza dei quattro esperimenti principali del CERN: ATLAS, ALICE, LHCb e CMS. Grazie alle alte energie raggiunte, che ancora fanno di LHC il primo e unico acceleratore al mondo in grado di ricreare tali condizioni, non solo è possibile testare i modelli teorici alla base della descrizione delle interazioni fondamentali della materia, ma anche ampliare la nostra conoscenza scientifica e medicale.

Il Gruppo di Criogenia, all'interno del quale si è svolto questo lavoro di tesi, è parte del dipartimento di Tecnologia del CERN e si occupa di tutti gli studi che trattano l'analisi del comportamento fisico, meccanico, elettrico e magnetico dei materiali alle basse temperature. Inoltre il Gruppo è responsabile del mantenimento a basse temperature degli oltre 1000 magneti superconduttori presenti nell'LHC. Questo fa dell'acceleratore il piú grande sistema criogenico al mondo, e la temperatura di 1.9 K alla quale è necessario sfreddare i magneti per renderli funzionanti, lo rende un luogo piú freddo dello spazio siderale, la cui temperatura è di 2.7 K (-270.5°C). Infatti niobio-titanio, il materiale di cui sono costituiti i magneti, deve essere operato a tali temperature per poterne sfruttare le proprietà superconduttive, temperature che, per poter essere raggiunte, necessitano di un circuito chiuso di elio liquido superfluido.

Il presente lavoro di tesi è stato richiesto al Gruppo di Criogenia dal gruppo responsabile dell'esperimento COMPASS (Common Muon and Proton Apparatus for Structure and Spectroscopy®) situato nella zona nord del CERN. COMPASS è un esperimento di fisica ad alta energia presso l'acceleratore SPS in cui circola un fascio di protoni a 450 GeV. Questo fascio primario viene al bisogno fatto incidere su un bersaglio fisso, in modo da produrre un fascio secondario costituito da muoni e protoni a 160 GeV. Dal fascio secondario, a seconda che si debbano condurre studi strutturali o di spettroscopia adronica, viene selezionato il fascio di muoni o di protoni rispettivamente, il quale viene infine indirizzato all'esperimento COMPASS. Qui, il fascio secondario interagisce con un bersaglio di materiale polimerico contenente idrogeno liquido, producendo particelle secondarie che possono essere tracciate e sudiate tramite rivelatori situati a valle del bersaglio, nella catena dell'esperimento (Fig.1).

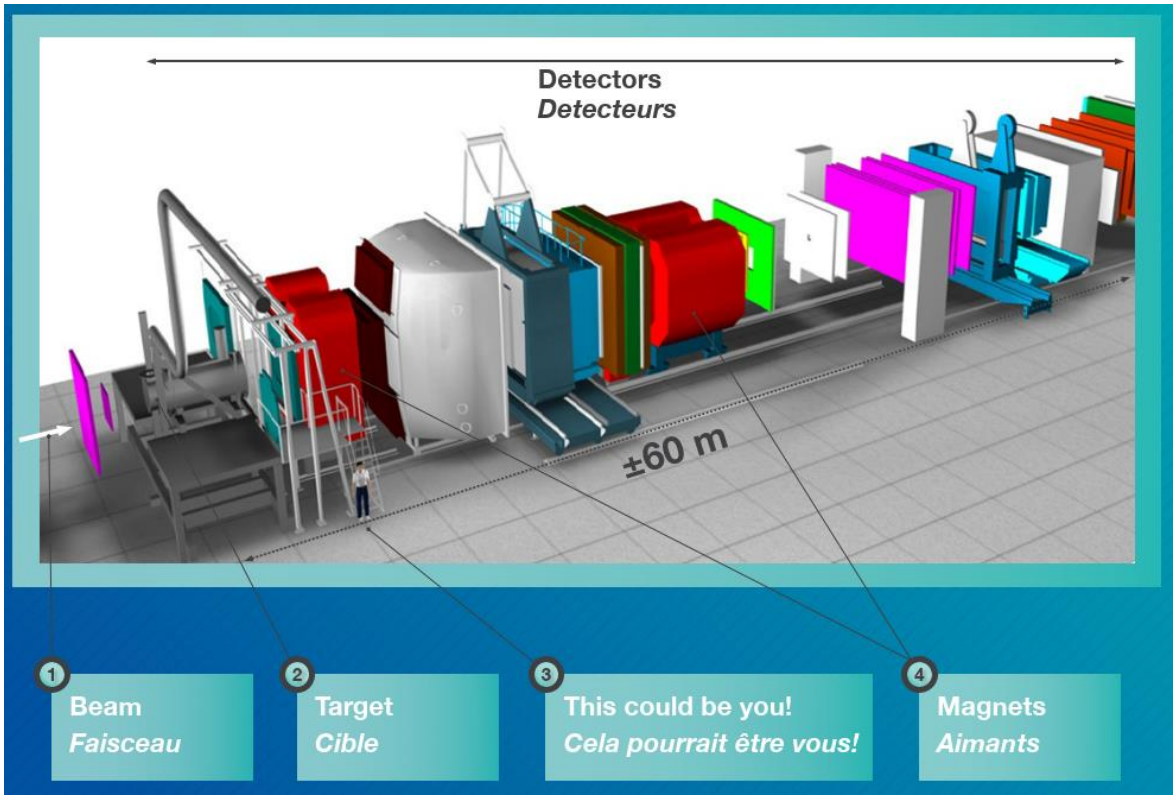

Fig. 1 – COMPASS experiment.

I vincoli sperimentali di COMPASS richiedono un bersaglio di idrogeno liquido con una lunghezza sensibile di 2.5 m ed un diametro di 0.04 m. Per ridurre il carico di calore del fascio sul bersaglio, esso è stato inserito in una camera a vuoto, e in modo da minimizzare l'interazione tra le particelle del fascio e le pareti del bersaglio e della corrispondente camera a vuoto, i materiali costituenti questi due elementi devono essere selezionati con cura: per le pareti del bersaglio si prediligono materiali polimerici, ragion per cui è stata scelta una lamina Kapton® dello spessore di 0.140 mm, avvolta a tubo e incollata su un lato a un cappuccio preformato in Mylar®, mentre sull'altro lato è stata incollata su un anello in acciaio inossidabile attraverso cui entra l'idrogeno liquido.
Durante questo secondo long shutdown di LHC, periodo nel quale tutti gli acceleratori sono spenti per permettere lo studio di migliorie e analisi dei dati, il team dell'esperimento COMPASS ha appunto richiesto al Gruppo di Criogenia l'analisi di diversi tipi di polimeri potenzialmente atti a sostituire i materiali costituenti il bersaglio, al fine di migliorarne la prestazione. Sono quindi stati realizzati dei campioni con i polimeri scelti come candidati e si è proceduto allo studio di permeazione e diffusione dell'idrogeno e dell'elio su tali campioni, a diverse pressioni di iniezione e a diverse temperature. Lo scopo è quello di ricavare una dipendenza dalla temperatura della permeazione, cercando il campione meno permeante a basse temperature. Si noti che a causa di limiti strutturali dell'apparato sperimentale, la temperatura minima usata nelle misure presentate in questa tesi è stata 142 K, ben al di sopra della temperatura di esercizio di COMPASS di 20 K. Nonostante ciò, dai set di misure effettuate a piú alte temperature è possibile inferire il valore di permeazione alle temperature di lavoro di COMPASS. Lo studio è stato fatto su tre campioni polimerici realizzati con DuPont Kapton HN. L'impianto di permeazione è costituito principalmente da un criostato che, al suo interno, presenta due camere mantenute a pressione diversa e

affacciate al campione. Una volta inserito il campione, nelle due camere viene pompato il vuoto mediante due pompe per lato, collegate in serie: una rotativa per il pre-vuoto e una turbomolecolare, con la quale si raggiunge un vuoto spinto finale dell'ordine di 10^{-8} mbar. Si procede poi abbassando la temperatura dell'impianto: all'interno del criostato è presente una piastra termica per regolare la temperatura e dei sensori per monitorare le variazioni di temperatura e pressione. Raggiunta la temperatura desiderata si procede iniettando da una delle due camere il gas oggetto di studio che, per uscire, potrà passare solo attraverso il campione. Nella camera posta al di là del campione viene accumulato il gas che è permeato, monitorandone il volume. Sono state effettuate misure di due tipi: una statica, che è appunto quella ottenuta misurando la pressione nella camera al di là del campione la quale, nota la geometria dell'impianto, permette di calcolare la quantità di gas permeato; la seconda misura è di tipo dinamico, ottenuta aprendo la camera al di là del campione e misurando il flusso di gas che fuoriesce tramite un Residual Gas Analyser (RGA). La misura dinamica ha lo scopo di verificare il risultato di quella statica, ovvero da entrambe si dovrebbe ottenere lo stesso risultato. Per ogni campione si è proceduto allo stesso modo: prima si è iniettato il gas con massa atomica minore, l'idrogeno, e successivamente quello con massa maggiore, l'elio. L'idrogeno è stato iniettato a tre diverse pressioni, rispettivamente 600 mbar, 800 mbar e 1 bar, per ogni valore di temperatura, ovvero 179 K, 197 K e 226 K. Per quanto riguarda l'elio, non trattandosi di un test richiesto espressamente da COMPASS, esso è stato iniettato alla sola pressione di 800 mbar ma per piú valori di temperatura, rispettivamente 142 K, 179 K, 197 K, 226 K e 250 K. In seguito, per ogni campione si è proceduto all'analisi dei dati: tramite le due leggi di Fick si sono ricavati i coefficienti di permeazione di ogni singola misura statica, i quali, tramite l'equazione di Arrhenius, sono esprimibili in funzione dell'inverso della temperatura. Si crea cosí una dipendenza biunivoca tra il valore di permeazione e la temperatura: sostituendo in tale equazione la temperatura di esercizio di COMPASS ed essendo noti gli altri parametri possiamo ricavare il coefficiente di permeazione a tale temperatura.
Sulla base dei risultati ottenuti si è quindi valutato quale campione presentasse il minor valore di permeazione, essendo tale la caratteristica richiesta al materiale sostitutivo per il bersaglio di COMPASS.

Contents

1 Introduction

1.1 CERN

The European Organization for Nuclear Research (CERN) is an international research center located on the Franco-Swiss border near Geneva. Its creation born from the idea of a little number of visionary scientists in Europe and North America that felt the need for Europe to have a world class physics research facility. Their vision was both to stop the brain drain to America that had begun during the Second World War, and to provide a force for unity in post-war Europe. In this way, in December 1951 at an intergovernmental meeting of UNESCO was adopted the first resolution concerning the establishment of a European Council for Nuclear Research (in French *Conseil Européen pour la Recherche Nucléaire* – CERN). In June 1952, the final draft of the CERN convention was agreed upon and signed by 12 new Member States. It laid out the ways Member States would contribute to CERN's budget, as well as early indications of CERN's ethos and organization, from adopting a policy of open access, to CERN's internal structure being divided into directorates. In July 1955, Felix Bloch, CERN's Director-General, laid the first foundation stone. From the beginning CERN focused to uncover what the universe is made of and how it works. CERN is made up of a unique range of particle accelerator facilities: each machine increases the energy of a beam of particles, before injecting the beam into the next machine in the sequence. A view of the entire complex of accelerators is shown in Fig. 1.1:

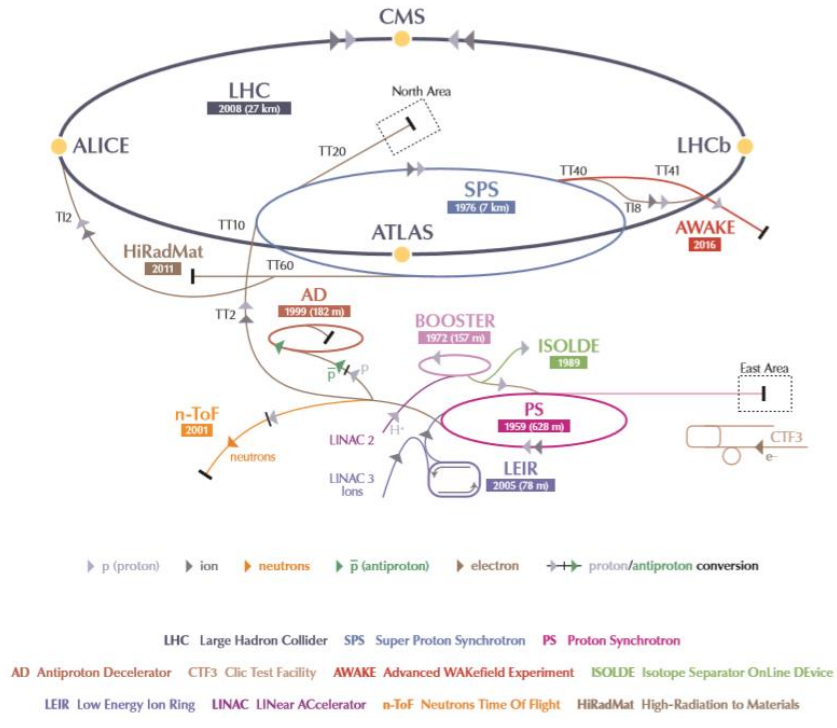

Fig. 1.1 – CERN accelerators facilities.

The proton source is a bottle of hydrogen gas: an electric field ionizes hydrogen atoms from their electrons to yield protons. Linac 2 is the first accelerator in the chain, it accelerates the

protons to the energy of 50 MeV; then the beam is injected into the Proton Synchrotron Booster (PSB), which accelerates the protons to 1.4 GeV, followed by the Proton Synchrotron (PS) which pushes the beam to 25 GeV. The protons proceed in the Super Proton Syncrotron (SPS) where they are accelerated to 450 GeV and then they are finally transferred to the two beam pipes of the Large Hadron Collider (LHC): here the beam in one pipe circulates clockwise while the beam in the other pipe circulates anticlockwise. It takes 20 minutes for the protons to reach their maximum energy of 6.5 TeV. The two beams are brought into collision inside four detectors which are ALICE, ATLAS, CMS and LHCb, where the total energy at the collision point is equal to 13 TeV.
This amount of energy can recreate the conditions of the first nanoseconds after the Big Bang, giving us the possibility to confirm physics theories and to improve the scientific knowledge.
The accelerator complex includes the Antiproton Decelerator (AD), the Online Isotope Mass Separator (ISOLDE) facility, the Compact Linear Collider test area and the neutron Time-Of-Flight facility (nTOF).
It's important to say that the results, the discoveries and the technological improvements deployed at CERN are not important just for the world of Physics and Scientists, in fact many times they have been extended to pratical and everydays life issues, especially in medical field.

1.2 COMPASS and its target chamber

The Common Muon and Proton Apparatus for Structure and Spectroscopy® (COMPASS) is a high-energy physics experiment at the Super Proton Synchrotron (SPS) at CERN.
Summarized from [1], the purpose of this experiment is the study of hadron structure and hadron spectroscopy with high intensity muon and hadron beams at 160 GeV. On February 1997 the experiment was approved by CERN and the final Memorandum of Understanding was signed in September 1998. The spectrometer was installed in 1999–2000 and commissioned during a technical run in 2001. The physics experiments started in summer 2002 with a muon beam and polarised proton and deuteron targets. These semi-inclusive deep inelastic scattering (SIDIS) experiments reveal details of the quark-gluon structure of the nucleon, in particular the gluon polarisation and transverse-momentum-dependent correlations. After the shutdown in 2005, COMPASS resumed the SIDIS experiments in 2006 and 2007 with a new large-aperture target magnet. The spin structure measurements were continued in 2010 and 2011. The years 2008 and 2009 were dedicated to the hadron spectroscopy programme with pion and proton beams scattering off a liquid hydrogen target and nuclear targets. An unprecedented amount of data was collected and has allowed for a much refined analysis of the final states, and is still revealing subtle details of the light-meson spectrum. Part of 2009 was dedicated to the study of the pion polarisability using Primakoff scattering of pions from heavy nuclei. This measurement had been prepared by a pilot run in 2004. The programme was continued in 2012 under COMPASS phase-II. Phase-II of COMPASS is primarily dedicated to the transverse and 3D structure of nucleons using Deeply Virtual Compton scattering (DVCS), Hard Exclusive Meson Production (HEMP), SIDIS and polarised Drell-Yan (DY) reactions. Approved in 2010, it started in 2012 with a Primakoff run and a DVCS pilot run using a muon beam and a long liquid hydrogen target with a huge recoil detector. The first-ever polarised Drell-Yan measurement with a beam of negative pions and a polarised proton target was successfully performed in 2015 and the data taking was resumed in 2018. The years 2016 and 2017 were dedicated to DVCS measurement and simultaneously data on HEMP and SIDIS were collected. For 2021 after

long shut-down 3, further measurements of SIDIS off transversely polarised deuterons were approved.
About 200 physicists from 13 countries and 25 institutions work in COMPASS [1].
The experimental constraints have asked for a liquid hydrogen target with a sensitive length of 2.5 m and a diameter of 0.040 m. To diminish the heat load to this target, it has been placed in a vacuum enclosure. The particles created or scattered in the liquid hydrogen volume shall be detected by the camera detector situated around the hydrogen target set-up. To reduce the interaction between the particles mentioned above and the walls of the hydrogen target and its corresponding vacuum enclosure, the construction materials of these two items have to be selected carefully. For the target walls a Kapton® foil strip, wound and glued to a thickness of 140 μm, has been selected. This Kapton® tube has been cut to the correct length and has at one side been glued to a pre-formed Mylar® end-cap, while the other side has been glued to a stainless-steel ring to which the liquid hydrogen entry, as well as the gaseous hydrogen return pipe have been connected.
The target is shown in Fig. 1.2.

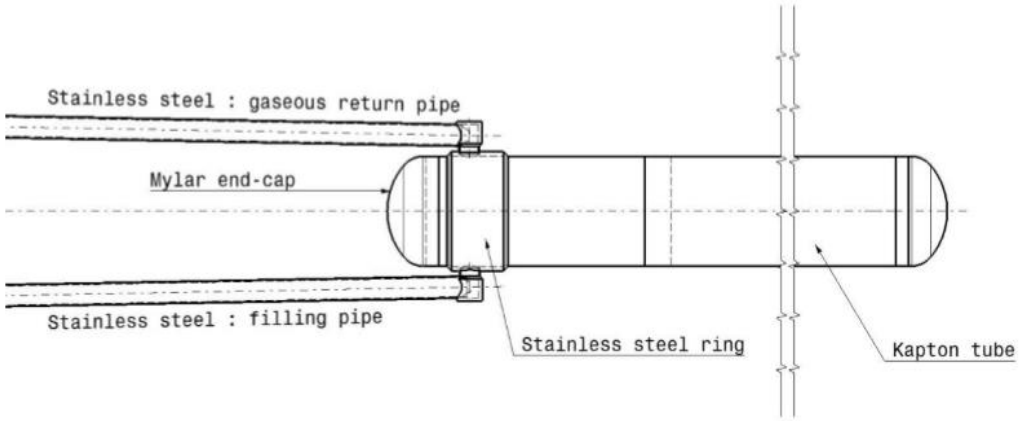

Fig. 1.2 – Design of COMPASS target from [2].

These pipes are also used for centering the Kapton® tube with respect to the beam line. The other side of the stainless-steel ring, the side from which the particles enter the hydrogen target, is also enclosed by a pre-formed Mylar® end-cap. In this way a sensitive liquid hydrogen volume of about 3.3 l has been created. During normal operation, the target volume has a maximum working pressure of 2 bar abs.
The liquid hydrogen target itself is placed in a 2.6 m long cylindrical vacuum enclosure formed by a 0.001 m thick Carbon Fiber Reinforced Plastics (CFRP) tube with an 0.08 m diameter (see Fig. 1.3). At the beam outlet side, an end-cap is mounted to the tube. This end-cap is constructed from a 0.002 m thick CFRP tube, closed by a 0.00035 m thick Mylar® foil.

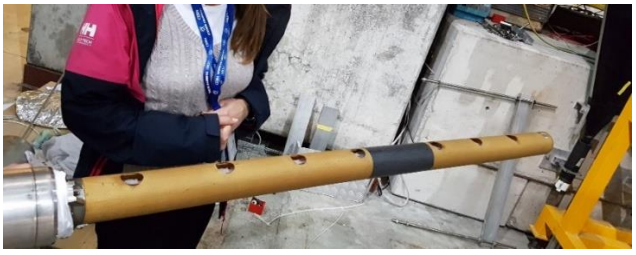

Fig. 1.3 – Picture of the COMPASS target.

The beam entrance side of the tube (see Fig. 1.4 and Fig. 1.5) is connected, via a flange connection, to a stainless-steel T-piece. At the top of this T-piece, the cryogenic system used for the cooling of the liquid hydrogen target is installed, while the other leg of this T-piece, where the beam enters, the experiment is closed by a 175 μm thick Mylar® foil mounted between two flanges [2].

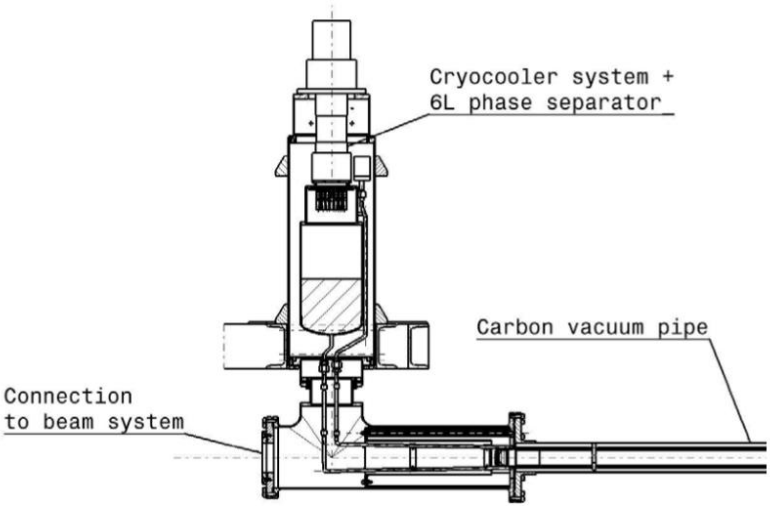

Fig. 1.4 – Vacuum enclosure and cryocooler installation from [2].

Fig. 1.5 – Central cryostat and its vacuum enclosure of COMPASS target.

1.3 Polymers in Ultra High Vacuum

Permeation and diffusivity of gases in polymers are topics of interest for many fields of application. Their importance is evident because these materials are largely used in different ways for their gas barrier and gas separation properties. Indeed, polymers with high barrier function are required for packaging of carbonated soft drinks and food in general, where the permeation of carbon dioxide, oxygen and water should be avoided.
In particular, polymers present many attractive properties in view of potential application in cold UHV system: they are easily moldable, light and resistant, electrical insulators and they are transparent to sub-nuclear particles and radiation. Unfortunately, in comparison with metals, their use is limited by a strong degassing of small molecules, mostly water, and gas permeation when they are exposed to a pressure difference [3 - 6].
A possible solution to reduce permeation consists of metallic coating on a polymeric substrate, combining mechanical properties of polymers and vacuum properties of metals [7, 8].

1.4 Polymers in CERN accelerator experiments

Polymers could be a good choice to make beam-pipes for accelerator experiments. They have to hold a good mechanical strength and a low atomic number in order to allow particles to reach the sensitive detector volume. Nowadays beryllium is the most common choice in this field for its transparency and good mechanical properties, but it shows some issues [6]:

- It is extremely toxic to lung tissue: this makes it very difficult and expensive its manufacturing and handling;
- It is very expensive: e.g. 50.000$/m per tube with 0.06 m of diameter;
- It is not easy to connect beryllium with other metals.

Polymers are already used in some experiments either with or without a metallic coating: for example, Kapton foils have been used to make the Gas Electron Multiplier (GEM), as we can see in Fig.1.6, and the target for COMPASS experiment [9 - 11].

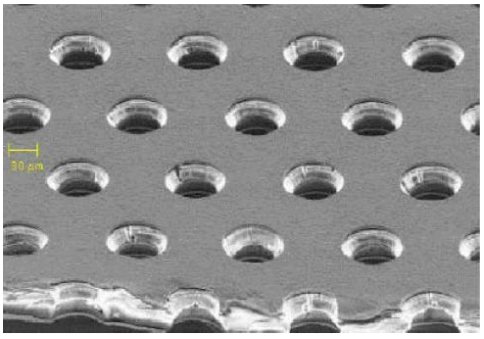

Fig. 1.6 – GEM applied: it is made by a Kapton membrane with a both side copper coating [5].

Moreover, PET windows have been used to decrease the background radiation in particles detector [12] and aluminized Mylar is used largely for the vacuum insulation in cryogenic systems [13].

2 Aim of the thesis

The aim of the thesis can be resumed in the following points:

- To study the dependence of the permeability and diffusivity coefficients of different polymers at low temperatures in order to understand their behaviours and properties;
- To evaluate the possibility to apply polymers in vacuum and at low temperatures;
- To find the best candidate for the new COMPASS target, between the polymers studied.

The study consists of:

1. Theoretical part:
   Thanks to the Fick's laws that describe the permeability and diffusion phenomena, it has been possible to get the solutions for the experimental conditions. Finally it has been possible to study both processes as function of the temperature through the Arrhenius' relationship.

2. Experimental part:
   For this aim, a remarkable number of permeation measurements have been made using two different methods in order to compare the results, in particular a static method and a dynamic one.
   With this measurements at low temperature it has been possible to show the permeability and diffusion dependence.

3 Theory

3.1 Vacuum

According to the American Vacuum Society, the term 'vacuum' refers to a given space filled with gas at pressure below atmospheric, i.e. having a density of molecules less than about 2.5E19 molecules/cm^3.
We can divide vacuum into three regions depending on the pressure of the gas:

- Low or rough vacuum (from the atmospheric pressure down to about 1E-05 mbar);
- High vacuum (1E-05 ÷ 1E-09 mbar);
- Ultra-high vacuum (below 1E-09 mbar).

Passing from a region to another, the technology that is used changes such as the choice of the materials, the surfaces treatment and the measurement methods.

3.1.1 Development of the vacuum technology

The first void was produced in 1644 by Torricelli (namesake of the first vacuum pressure scale 1 bar = 760 mmHg ~ 760 Torr), who identified it in the space not occupied by mercury in a glass cylinder closed at one end. Von Guericke (1602−1686) was the first to understand that air can be pumped directly like water; therefore, he designed the first pumps that were very similar to those for water suction [14].
In 1892 Fleuss developed a cylinder pump, Geryk pump, which reached 2E-04 Torr, parallel to which mercury pumps were developed, based on the continuous application of the Torricelli method and were used by Edison, in 1879, for the manufacture of the first incandescent lamp (1E-03 Torr). The year 1905 can be considered as the beginning of modern vacuum technology; its main supporter was certainly Gaede, who produced a new pump that reached 7E-05 Torr with mechanical pumping only. Meanwhile, the new concepts of kinetic theory began to enter into the vacuum technology.
It was still Gaede who introduced the molecular pump in 1912 and who in 1915 built the first diffusion pump, which subsequently allowed him to obtain pressures lower than 1E-08 Torr [14]. The same pump was then improved by Languimir and used for the first experimental physics and chemical studies. The great success of diffusion pumps delayed the improvement of molecular pumps by about 40 years. Only in 1958, in fact, Becker introduced the turbomolecular pump. A better knowledge of chemical bonds allowed, in the first half of the last century, to achieve a decisive step towards UHV: the removal of molecules from the gas phase by capturing them on a chemically active surface (gettering) [14].
Hence, the transition metals in vacuum technology, in particular titanium, were introduced and in 1953 the first ionic pumps were used for UHV production. The first titanium sublimation pumps and the cryopumps were introduced at the same time, allowing pressures of 1E-13 Torr to be obtained. In the 1950s, the barium getters made their entry, in the 1960s the porous non-evaporable getters made of zirconium alloys and in the 1980s the non-evaporable porous getter with low activation temperature [15].
No reference has been made so far to the measurement of the degree of vacuum. Briefly, we can say that the evolution of vacuum gauges has never anticipated that of pumping methods. Bayard and Alpert introduced the first vacuum gauge capable of

measuring pressures below 1E-09 Torr in 1950 [1]. Modern vacuum gauges, developed following the idea of Alpert, are able to measure pressures of the order of 1E-14 Torr.

3.1.2 How to create vacuum

Usually we start with air at atmospheric pressure in a chamber, which is connected to a vacuum pump. Air at atmospheric pressure is a combination of gasses, as shown in Tab. 3.1.

Tab. 3.1 – Air composition at 50 % relative humidity.

Gas	Percent
N_2	78.08
O_2	20.95
Ar	0.93
CO_2	0.033
Ne	1.8E-03
He	5.24E-04
CH_4	2.0E-04
Kr	1.1E-04
H_2	5.0E-05
N_2O	5.0E-05
Xe	8.7E-06
H_2O	1.57

The vacuum pump removes gas molecules from the chamber to reach the desired vacuum [16]. Gas molecules are always moving and colliding, molecule-to-molecule. The distance between molecules is a function of pressure and it is known as the mean free path (MFP): Gas molecules at atmospheric pressure are very close together, so the collisions are very often; as the chamber is pumped down into vacuum and molecules are removed, the MFP becomes greater and greater and this is explained in Fig. 3.1.

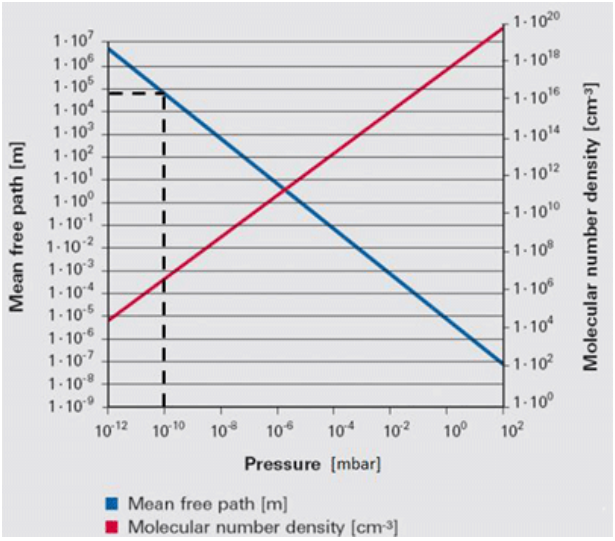

Fig. 3.1 – Molecular mean free path in [m] and Molecular number density in [cm^{-3}] as a function of pressure in [mbar] from [3].

As pressure decreases in a chamber, fewer molecules are present and the mean free path increases. In the same way, as the gas density reduces, there are fewer chances of molecular collision.
Air molecules can be removed from the chamber in different ways.

3.1.3 Vacuum units of measurements

Measuring vacuum requires standard units of measure, as shown in Tab. 3.2: mmHg, Torr and bar are three units of measure associated with the vacuum furnace industry, while for others fields of vacuum we use Pascal.

Tab. 3.2 – Units of vacuum measurement [3].

	mmHg	Torr	bar
1 mmHg	1	1	1.3E-03
1 Torr	1	1	1.3E-03
1 bar	750.062	750.062	1

3.1.4 How to measure vacuum

From the year 1644 to about 1900, the Torricelli tube was the only instrument able to measure vacuum. It was based on the counterbalance of the gravitational force of a mercury column against a pressure difference in two volume separated by the liquid mercury. If one of the volumes was under 'vacuum' conditions, it was an absolute instrument and pressure was measured in 'mmHg' and later in 'Torr' [17].
Unfortunately, these units are still being used today in some areas, even though the Torricelli tube is out of practical use and the *Conférence générale des poids et mesures* (CGPM) was implemented almost 50 years ago in 1960 when the Système International (SI) of physical units replaced the Torr by the Pascal. The Pascal (Pa) is the force of 1 newton on 1 m^2 as pressure in defined by the equation (3.1) [17]:

$$p = \frac{F}{A}. \tag{3.1}$$

The measurement of vacuum pressure follows equation (3.1) by a direct measurement of the force per area (direct gauge) or indirectly by measurement of a quantity that is proportional to pressure, for example the thermal conductivity.
The direct measurement of pressure is limited to pressure larger than about 1 mPa. At this pressure, the force on 1 cm^2 is only 1E-07 N which already needs an electrically amplified signal.
Classification schemes of vacuum gauges measuring pressure directly and indirectly respectively are shown in Fig. 3.2 and Fig. 3.3:

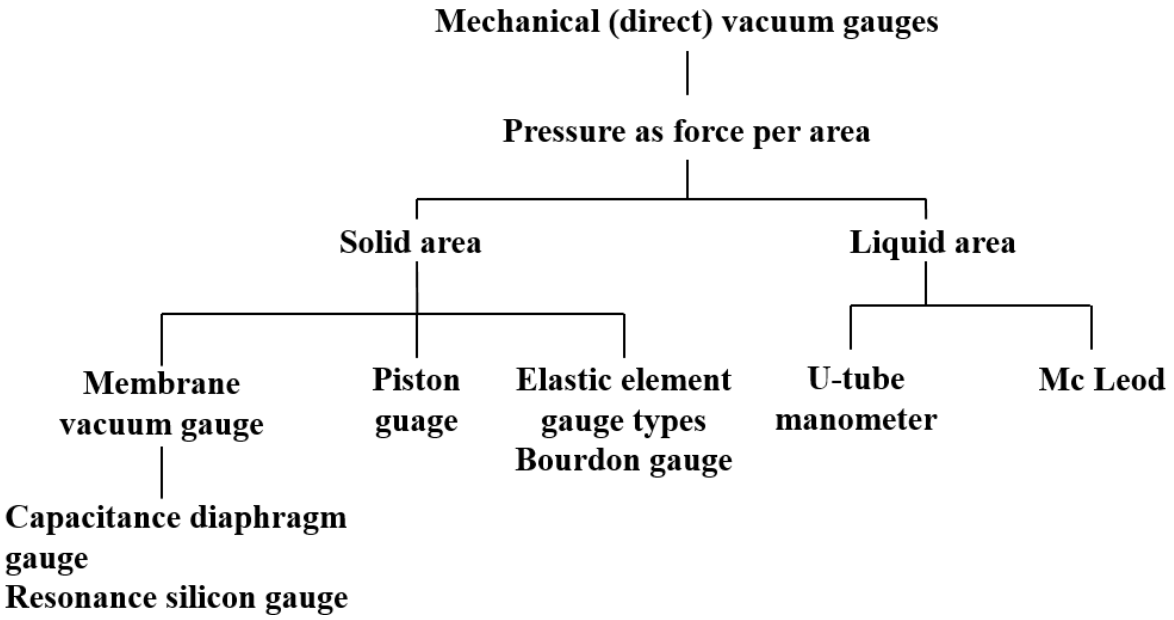

Fig. 3.2 – Classification scheme of direct vacuum gauges.

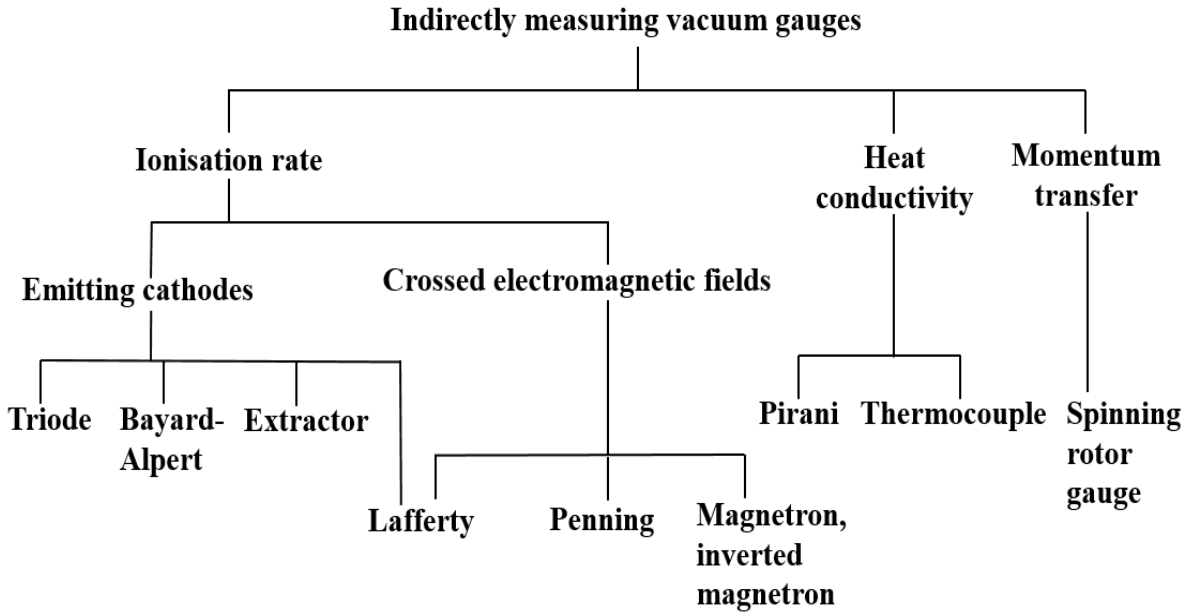

Fig. 3.3 – Classification scheme of indirect vacuum gauges.

The main characteristic of the direct gauges is that the reading is independent of the gas species: they truly measure a total pressure of a gas mixture or a pure gas. On the other hand, the signal of indirect measuring vacuum gauges depends for a given pressure on the gas species and for this reason it may not be possible to convert the signal onto a correct pressure reading if the gas composition of a mixture is not known exactly [17].

3.1.4.1 Mechanical gauge

Mechanical gauges are constituted by a membrane who detect the force of the pressure; this force is expressed following the equation (3.2):

$$F = (p_1 - p_2)A, \tag{3.2}$$

and it causes a deflection x of the membrane that can be used for measurement. In most cases x is converted into an angle φ that can be used for a needle indicator. When the reference pressure p_2 is negligible compared to p_1 the instrument shows the absolute pressure. The reference pressure is the atmospheric pressure and the measurement device is located on the reference side, it is zero when the measurement device is located on the other sine or on the same reference side [17].

3.1.4.2 Thermal conductivity gauge, Pirani

For a certain range of pressure, gas conducts thermal energy proportionally to the number of molecules involved in the transport. We can use this effect to measure vacuum pressures: the power loss of a heated element, usually a wire, to an enclosure of stable temperature is measured.
When we are at high pressure the gas density is so high and the mean free path of the molecules so short that the gas can be described as a continuum: there is also a heat flow from an element at higher temperature to a wall of lower temperature but it not depend on pressure.
At low pressure each molecule transports some energy and the total amount of energy transport is proportional to the number of molecules; in the intermediate regime the proportionality becomes weaker [17].
In the year 1906 Pirani invented a gauge that takes advantage of thermal conductivity; he put the heated wire as part of a Wheatstone bridge, which supplies the necessary electrical power. There are different operational modes: the most accurate gauges are those where the temperature of the heated element is held constant, they are expensive but with the largest measurement range. Otherwise, we can measure the temperature of the wire maintaining the heating voltage, current or power constant [17].
The reading of thermal conductivity gauges mainly depends on the gas species and its properties, like degrees of freedom, mean thermal velocity of the molecules but also it depends on the accommodation of the gas molecules on the respective surfaces. For this reason, thermal conductivity gauges are very sensitive to any pollution and one gas species dependent.

3.1.4.3 Ionization gauge

In the ultrahigh vacuum regime it is not possible to measure pressure as a force on a certain area as the definition of pressure indicates, nor the thermal conductivity. The only reasonable indicator for pressure is the ionization rate produced by electrons hitting the neutral gas atoms in a UHV chamber.
The measuring principle of an ionization gauge is shown in Fig. 3.4: when an electron that is emitted from cathode K, hits neutral molecules closely enough it may ionize them. The ions are drawn to the collector C, the electrons finally reach the anode A [18].

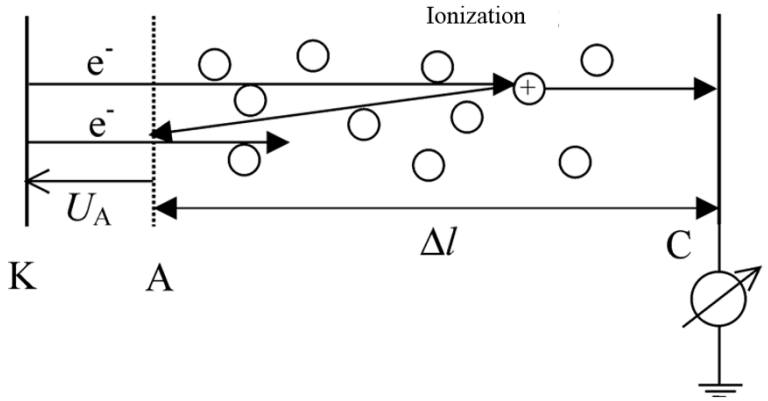

Fig. 3.4 – Ionization mechanism produced by electrons, from [17].

In the ionization gauges (IG), the ionization rate is proportional to the particle density *n* in the gauge volume. For this reason it is important to remember the ideal gas law for an enclosed system in equilibrium that follows the equation (3.2):

$$p = nkT. \tag{3.3}$$

To indicate a pressure with an IG one needs to measure n, with an ion gauge, and the temperature T of the gas.
It is possible to ionize neutral gas molecules by photons or ions, only the use of electrons is economically feasible [18].
There are two types of ionization gauges generated by the different production methods of electrons: when the electrons are generated by an electrical discharge, the gauges are usually called 'cold cathode gauges' while when the electrons are generated by a heated cathode, they are called 'hot cathode ion gauges' [18].

3.1.4.4 Penning gauge

It generates a discharge between two metal electrodes, the anode and cathode, by applying a DC high voltage. The discharge current is pressure dependent and serves as indicator for the pressure. The lower measurement limit lies around 1 Pa, since at lower pressures the gas density is too low to generate enough charge carriers to maintain the discharge [18].
To increase the pressure range, we need a magnetic field that crosses the electrical field: in a way that the magnetic field increases the path length of the electrons from the cathode to anode and electrons can generate another electron by impacting on a gas molecule to maintain the discharge. Because of the higher mass the ions are not so much affected in their trajectories by the magnetic field and they travel directly to the cathode.
Secondary electrons are then released when the ions hit the cathode support the discharge.
In crossed field gauges, the ion current versus pressure relation follows the equation (3.4):

$$I^+ = K * p^m, \tag{3.4}$$

where m depends on the type of gauge and varies between m = 1… 1.4.
In the following Fig. 3.5 the mode of operation in a penning discharge is described: The typical range of a penning gauge reaches therefore 1E-03 mbar to 5E-10 mbar.

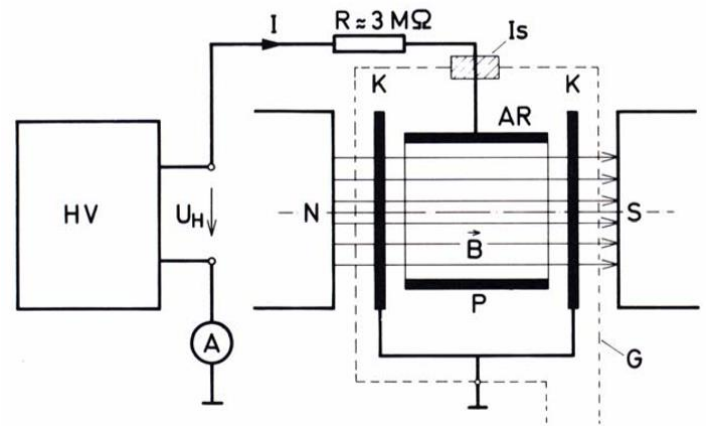

Fig. 3.5 – Scheme of a penning gauge, where AR is anode ring, K cathode, G case, N, S north and south pole of magnet, HV high voltage [19].

3.1.5 Vacuum application

In a closed volume, at room temperature, the pressure directly defines the molecular density, the average free path and the rate of collisions on a surface. Assuming that for each impact a molecule is adsorbed, it is also possible to define the development time of an adsorbed gas monolayer (see Tab. 3.3).

Tab. 3.3 – Variations of the molecular density, the average free path and the development of a monolayer as function of the pressure.

Pressure [Torr]	Density [cm^{-3}]	Mean free path [cm]	Development of a monolayer [s]
1	3.2E+16	5.3E-03	1.5E-06
1E-03	3.2E+13	5.3	1.5E-03
1E-06	3.2E+10	5.3E+03	1.5
1E-09	3.2E+07	5.3E+06	1.5E+03
1E-12	3.2E+04	5.3E+09	1.5E+06
1E-15	3.2E+01	5.3E+12	1.5E+09

The large variety of applications of vacuum can be classified either according to the physical situation achieved by vacuum technology or according to the fields where the application belongs, as it is described in the Tab. 3.4 [20].

Tab. 3.4 – Applications of vacuum techniques.

Physical situation	Objective	Applications
Low pressure	Achieve pressure difference	Holding, lifting transport (pneumatic, cleaners, filtering), forming
Low molecular density	Remove active atmospheric constituents	Lamps (incandescent, fluorescent, electric discharge tubes), melting, sintering, packaging, encapsulation, leak detection
	Remove occluded or dissolved gas	Drying, dehydration, concentration, freeze drying, degassing, lyophilisation, impregnation
	Decrease energy transfer	Thermal insulation, electrical insulation, vacuum microbalance, space simulation
Large mean free path	Avoid collisions	Electron tubes, cathode ray tubes, television tubes, photocells, photomultipliers, x-ray tubes, accelerators, storage rings, mass spectrometers, isotope separators, electron microscopes, electron beam welding, heating coating (evaporation, sputtering), molecular distillation
Long monolayer formation time	Clean surfaces	Friction, adhesion, emission studies, materials testing for space

3.1.3 Beam Vacuum

CERN uses vacuum in many ways for the accelerators and their experiments; just for the LHC, we have three vacuum systems:

- Insulation vacuum for cryomagnets and cavities;
- Insulation vacuum for helium distribution line (QRL);
- Particle beam vacuum.

In particular, the beam vacuum is necessary to reduce drastically collisions with gas molecules; it is an ultrahigh vacuum at a pressure smaller than 1E-13 bar and it is used in every part where the beams propagate in accelerators.

3.2 Diffusivity in Polymers

3.2.1 Diffusion

The term diffusion stands for the movement of particles in a solid, from an area of high concentration to an area of low concentration, resulting in the uniform distribution of the substance.
It is the result of the random movements of atoms (statistical problem) and factors which influence diffusion, including:

1. The molecular size and physical state of the diffusant;
2. The morphology of the porous material;
3. The compatibility or solubility limit of the solute within the polymer matrix;
4. The volatility of the solute;
5. The surface of interfacial energies of the monolayer films.

3.2.2 Diffusion Equations

In the year 1855 Fick proposed the law of mass diffusion, better known as Fick's first law [21]. The mathematical expression of this law is shown in the equation (3.4):

$$J = -D\nabla c, \tag{3.4}$$

where J is the flux, defined as the amount of gas which passes per unit area of section per unit of time. ∇c is the gradient of the concentration of diffusing substances and D is the diffusion coefficient.
Using the mass-balance of the equation (3.5):

$$\nabla J = -\frac{\partial c}{\partial t}, \tag{3.5}$$

one can combine it with the Fick's first law (3.4) and it has been possible to obtain Fick's second law, expressed as in the equation (3.6):

$$\frac{\partial c}{\partial t} = D\nabla^2 c. \tag{3.6}$$

With specific initial or boundary conditions this type of partial differential equations can be solved and one can give the concentration as function of special position and time c(x,y,z,t). The dependence of gas diffusion on temperature is expressed in terms of an Arrhenius type relationship, as movement of gas molecules through a membrane is considered a thermally activated process; following the equation (3.7) [22]:

$$D = D_0 e^{-\frac{E_d}{RT}}, \tag{3.7}$$

where E_d is the diffusion activation energy and D_0 is a constant independent of temperature. The activation energy is dependent on the size of the permeant.

3.2.3 Activation Energy

To spread out through the material the gas molecules have to overcome a certain activation energy E_a and enter in a reactive state, as we can see in Fig. 3.6; only a fraction of the entire molecules that constitute the gas have sufficient energy to reach E_a.

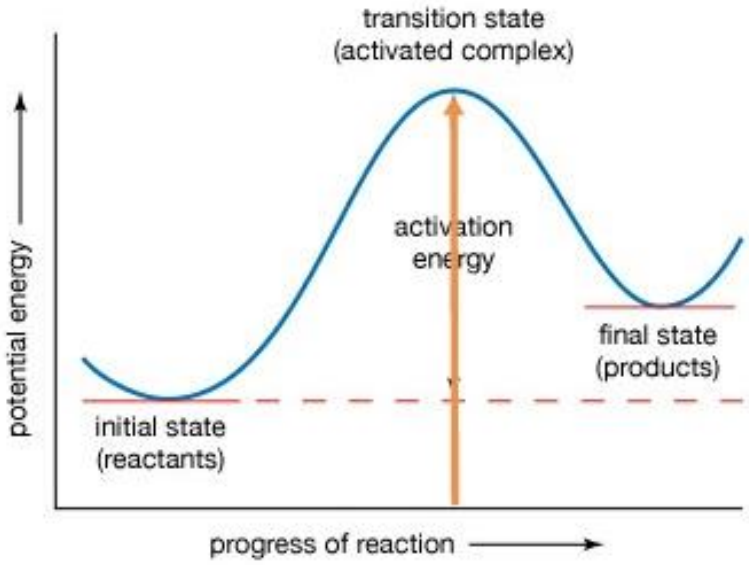

Fig. 3.6 – Activation energy, from [23].

The Arrhenius equation in terms of rate constant, shown in the equation (3.8), allows us to calculate activation energies if the rate constant is known or vice versa:

$$K = Ae^{-\frac{E_a}{RT}}, \tag{3.8}$$

where K represents the rate constant, E_a is the activation energy, R is the gas constant (8.3145 J/K mol), and T is the temperature expressed in Kelvin. A [l $mol^{-1}s^{-1}$] is known as the frequency factor and takes into account the frequency of reactions and likelihood of correct molecular orientation. This equation mathematically expresses that as activation energy term E_a increases, the rate constant K decreases and therefore the rate of reaction decreases [23]. Each phenomena through the sample needs an activation energy of molecules, in fact one has E_d for the diffusion and E_k for the permeation.

3.3 Solubility in polymers

The solubility *S* of a molecule in a polymer is normally defined, under conditions of thermodynamic equilibrium, by the following equation (3.9):

$$S = \frac{c}{p}, \tag{3.9}$$

where c and p are the gas concentration and pressure, respectively. The thermal effects on solubility and diffusion show opposite trends in polymers. Generally, for gas adsorption, solubility decreases with increase temperature due to the condensability of the penetrant at lower temperatures.
The solubility dependence with temperature is typically written in terms of the Van't Hoff relationship, following the equation (3.10) [24]:

$$\frac{d(lnS)}{dT} = \frac{\Delta H_S}{RT^2}. \tag{3.10}$$

where ΔH_s is the partial molar enthalpy of sorption.
Integrating equation (3.10) results in:

$$S = S_0 e^{-\frac{\Delta H_S}{RT}}, \tag{3.11}$$

where S_0 is a constant independent of temperature.
In thermodynamics the solution is a two-step process: The first step involves the condensation of the gas molecules in a polymer, followed by creation of a molecular scale "hole" for accommodating the gas molecule. These individual steps contribute to the total enthalpy of sorption and are mathematically expressed as equation (3.12):

$$\Delta H_s = \Delta H_{cond} + \Delta H_{mix}, \tag{3.12}$$

where ΔH_{cond} is the enthalpy of condensation and, of course, it is always negative. Its presence is justified by the fact that the gas molecules, accommodated in the "hole", are closely surrounded by other gas molecules as in liquid state. ΔH_{mix} is defined as the enthalpy after the mixing minus the enthalpy of pure solute and solvent.
Depending by the interaction between gas and polymer, this energy could be positive or negative. For low molecular weight super critical gases, low condensation enthalpy causes the mixing enthalpy to control the sorption property of a polymer.
This means that for repulsive interactions between the gas molecule and the polymer, the enthalpy of sorption is positive so an increase of temperature leads to an increase of solubility.

For the case of condensable gases and vapours, the enthalpy of condensation dominates the process, thereby showing decreasing solubility with increasing temperature [24], as we can see for example in Fig. 3.7:

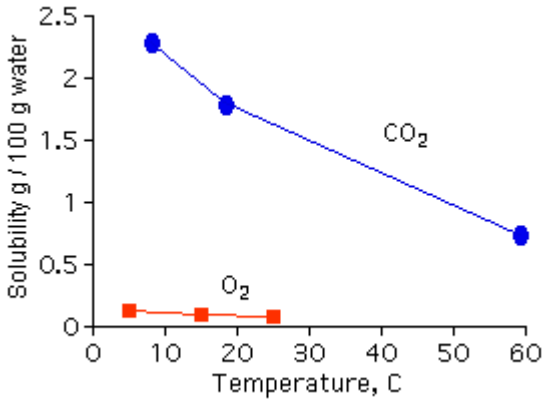

Fig. 3.7 – Solubility of gases versus temperature, from [23].

3.4 Permeability in polymers

3.4.1 Steady state condition

Let us study a flat polymeric sample with a thickness *l* and surface *A*, as it is shown in Fig.3.8:

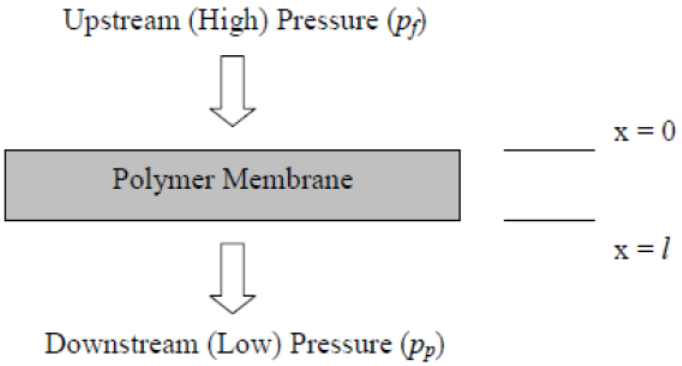

Fig. 3.8 – Scheme of gas transport through a polymeric membrane, from [6]..

The steady state condition assumes that the diffusant concentration remains constant at all points on each side or surface of the membrane. Hence, providing that the diffusion coefficient is constant and considering that the gas flows only perpendicularly through the membrane along the x direction, Fick's second law of diffusion reduces to equation (3.13):

$$\frac{d^2c}{dx^2} = 0. \tag{3.13}$$

Integrating this equation twice in respect to *x* and introducing the boundary conditions at *x*=0 and *x*=l, we obtain the equation (3.14):

$$\frac{c-c_{hp}}{c_{lp}-c_{hp}} = \frac{x}{l}, \tag{3.14}$$

where c_{hp} and c_{lp} are the concentration on the high pressure and on the low pressure side, respectively.
The concentration changes linearly from c_{hp} to c_{lp} through the membrane and the rate of transfer for a diffusing substance is the same across all sections. Therefore, we can calculate the rate of transfer per unit area of cross section by the following equation (3.15):

$$J = \frac{D(c_{hp}-c_{lp})}{l}. \tag{3.15}$$

In systems where a gas or vapour is the diffusant, the surface concentration cannot be known easily. In gas and vapour systems, the rate of diffusant transfer is expressed in terms of vapour pressures through the equation (3.16):

$$J = \frac{K(p_{hp}-p_{lp})}{l}, \tag{3.16}$$

where K is the permeability coefficient.
If we assume the diffusion coefficient as a constant, the relationship between the diffusion coefficient, the permeation coefficient and the solubility coefficient can be written as in the equation (3.17):

$$K = DS. \tag{3.17}$$

Finally, if the rate of diffusion is empirically determined and the solubility coefficient for the diffusant is known, the permeation and diffusion coefficients are easily calculated from equation (3.17).

3.4.2 Non-steady-state condition

Given the fact that during the permeation measurement the gas concentration changes on both sides of the sample, it could be interesting to study how the concentration changes for the time of all the process. We assume, during the measures, that the diffusion is in one direction through a sample which has as extremities two flat and parallel surfaces (x=0, x=l). Over time, the concentration of gas molecules assumes different values on the two sides of the samples: c_{hp} is the concentration in x=0 due to the injection of gas, c_{lp} lower than c_{hp} and that we can approximate to zero when we start measuring, is the concentration on surface x=l. The initial concentration c_0 inside the sample is close to zero. The Fick's second law of diffusion written as in the equation (3.13) gives the development of the concentration through the polymer, as it is shown in equation (3.18) following the description from [25]:

$$c = c_{hp} - c_{hp}\frac{x}{l} - \frac{2}{\pi}\sum_{n=1}^{\infty}\left(\frac{c_{hp}}{n}\right)\sin\left(\frac{n\pi x}{l}\right)e^{-\left(\frac{Dn^2\pi^2 t}{l^2}\right)}. \tag{3.18}$$

If one defines M_t the amount of gas which is inside the membrane with the time, following the equation (3.15),

$$M_t = \int_0^l c dx \,, \tag{3.19}$$

and one combines the two equations, one gets:

$$\frac{M_t}{M_\infty} = 1 - \frac{8}{\pi^2}\sum_{n=0}^{\infty}\frac{1}{(2n+1)^2}e^{-\left(\frac{D(2n+1)^2\pi^2 t}{l^2}\right)}, \tag{3.20}$$

where M_∞ is the amount of gas after an infinite time (steady-state condition).

Moreover, throughout the second Fick's law we obtain:

$$\frac{J_t}{J_\infty} = 1 + 2\sum_{n=1}^{\infty}(-1)^n e^{-\left(\frac{Dn^2\pi^2 t}{l^2}\right)}, \tag{3.21}$$

where J_∞ is the gas flux at steady state.
Integrating equation (3.21) respect to variable *t*, we obtain:

$$Q_t = lc_{hp}\left(\frac{Dt}{l^2} - \frac{1}{6} - \frac{2}{\pi^2}\sum_{n=1}^{\infty}\frac{(-1)^n}{n^2}e^{-\left(\frac{Dn^2\pi^2 t}{l^2}\right)}\right), \tag{3.22}$$

that is the amount of gas which passed the membrane until time *t*.
If $D\pi^2 t \gg l^2$, one can simplify equation (3.22) following [26] to:

$$Q_t = \frac{Dc_{hp}}{l}\left(t - \frac{l^2}{6D}\right). \tag{3.23}$$

Estimating the intercept in the last Q_t equation (3.23) on the time axis:

$$t = \frac{l^2}{6D}, \tag{3.24}$$

where *t* is called 'time constant', it is used to estimate the diffusion coefficient *D* from experimental data [27], [28], [29] and *l* is the thickness of the sample.

3.4.3 Temperature effects on permeability

Combining the temperature dependence for the diffusion and sorption coefficients with the equation (3.13), one obtains the temperature effect on gas permeability, expressed as in the equation (3.25):

$$K = K_0 e^{-\frac{E_k}{RT}} \tag{3.25}$$

Where E_k is the activation energy of permeation and is an algebraic sum of E_d and ΔH_s. In general, permeability increases with increasing temperature.

3.5 Cryogenics

Cryogenics is the branch of physics that deals with the production and effects of very low temperatures. Inside the Technology Department of CERN, there is a Cryogenics Group which supports the studies about the physical, mechanical, electrical and magnetic properties

of the materials at very low temperatures. Its task is very important here at CERN for many reasons, between these because the NbTi material of which the magnets of LHC are made it has to be maintained at very low temperature in order to take advantage of its superconducting properties: without cryogenics this wouldn't be possible.
In order to maintain the magnets to their work temperature of 1.9 K, a closed circuit with superfluid LHe: cooling is established thanks to this temperature LHC is considered a place coldest of the sidereal space whose temperature is 2.7 K (-270.5°C). Helium is chosen as refrigerant fluid for its particularly good properties when it reaches 2.17 K and becomes superfluid: it has a very high thermal conductivity, it is an efficient heat conductor and especially it allows to cool over long distances.
In addition to cooling superconducting magnets, cryogenic techniques are also used in particle detectors to keep heavy gases such as argon or krypton in a liquid state, for detecting particles in calorimeters or as particle targets such as for the COMPASS experiement.
The term *Cryostat* is generally employed to describe any container housing devices or fluids kept at very low temperatures; the notion of 'very low temperature' generally refers to temperature that are well below those encountered naturally on Earth, typically below 120 K. The very first cryostats were used in the pioneering years of cryogenics as containers for liquefied gases. The invention of the first performing cryostat is generally attributed to Sir James Dewar and hence cryostats containing cryogenic fluids are nowadays also called Dewars. In 1897 Dewar used silver-plated double-walled glass containers to collect the first liquefied hydrogen.
Even though the heat transfer phenomena were not well mastered during his époque, Dewar understood the benefits of thermal insulation by vacuum pumping the double-walled envelope, as well as shielding thermal radiation by silver-plating the glass walls.
H. Kamerlingh Onnes further developed glass-blowing, which became the enabling technology for making dewars for his laboratory in Leiden. He introduced this technique as one of the specialities in the school of instrumentation he founded, the Leidse instrumentmakersschool, which still exists today.
Since those times, the evolution of cryostats has been led by specific needs for the variety of applications. Today, cryostats can be found in a large range of applications spanning from industrial products to specific devices for scientific research instruments.
The basic function of a cryostat is to house and thermally insulate a low temperature device, while providing all the interfaces for its reliable and safe operation (cryogen feeding, powering, diagnostics instrumentation, safety devices, etc.).
The basic technical competencies for a cryostat design engineer are mechanical engineering and heat transfer. But their application at low temperatures calls for specific competencies on thermal and mechanical properties of materials at these low temperatures, which make the work very specific and a discipline by itself.
A cryostat is composed, as a minimum, of the following main components:

- Vacuum vessel
- Thermal shield
- Cryogenic vessels containing for example superconductor devices and/or containing cryogens
- Supporting systems

Vacuum and cryogenic vessels are sheet-metal constructions, with thicknesses typically in the 0.003 - 0.015 m range. Materials preferentially range from low-carbon construction steels

to stainless steels, though aluminium is also sometimes employed. Vacuum vessel materials operate at room temperature but must be qualified to withstand sudden cool down to about -70°C in case of accidental rupture of the insulation vacuum [30]. Qualification tests at low temperature have to demonstrate adequate energy absorption.
Cryogenic vessels are generally made of austenitic stainless steels. The austenitic structure does not undergo any ductile-to-brittle transition at low temperature and it is non-magnetic.
Thermal shields must be made of high thermal conductivity material. Copper and aluminium are the materials of choice, preferentially low alloyed for their better mechanical properties and manufacturability while still preserving good thermal conductivity. Pure coppers or aluminium are preferred only for demandingly high thermal conductivity where temperature homogeneity matters.
Materials for supporting systems usually depend on their design: they could be fibre-reinforced plastic materials, epoxy-based composites, injection-moulded plastics etc.

4. Setup, measurements and principles

4.1. Low temperature measurement system

In this paragraph, the set up will be discussed in which the measurements are performed. It is called ‘System 158’ and is mounted in the cryolab of CERN.
Fig. 4.1 shows the scheme of the set-up realized with AUTOCAD P&ID (piping and instrumentation diagram):

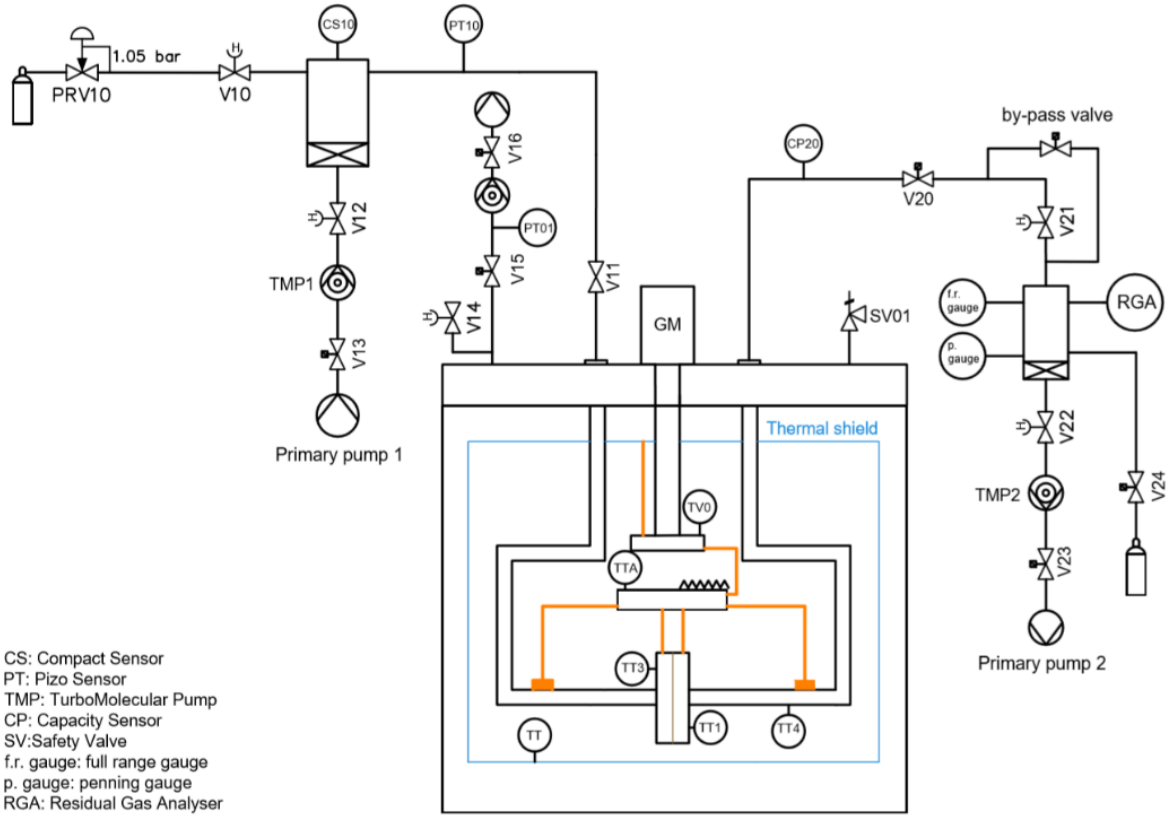

Fig. 4.1 – P&ID of the system, showing the cryocooler with its vacuum chamber hosting the cold part of the permeability set-up.

System 158 is constituted by a cryostat that works as a permeability cell. In fact, inside it has two channels which end with two chambers, around a sample. It is all surrounded by a thermal shield to thermally insulate the permeability process from outside and to maintain the operating temperature set by the intermediate block (TTA).
In the channel and the chamber upstream of the sample vacuum is pumped at a pressure of 1E-07 mbar and in it we inject the gas for the measurement; downstream of the sample, in the chamber and the channel vacuum is pumped at a pressure of 1E-08 mbar, and they serve to accumulate the gas that is permeated. Both channels continue outside the cryostat; in fact, the HP channel starts with a bottle from which one get the gas; it has a check valve in order to avoid a contamination of the pure gas inside the bottle and thus the valve has a pressure a little bit higher than atmosphere (1.05 bar, as it shown in the P&ID). Then the channel has a connection with a primary pump via a turbo molecular pump mounted in series and these are

essential to pump vacuum upstream the sample, for purging or to empty the channel from the residual gas of the previous measure (the same is present in LP side).
There is a piezo sensor PT10, which measures the quantity of gas that one is injecting; once I get the quantity of gas that I want to inject, I close the V11 valve to be sure to have upstream of the sample the exact desired quantity of gas during all the process.
The LP channel has a capacity sensor CP just outside the cryostat and it measures how much gas has been accumulated downstream the sample at V11 and V20 valves closed.
Then the channel continues with a by-pass valve that needs to evacuate fastly gas after measurements it is opened only after having measured the gas permeated with the Residual Gas Analyser (RGA); it is a dynamic measure that I can monitor with both the penning and the full range gauges. In the junction, where the RGA is collocated, there is also a connection to a helium calibrated leak, required for the RGA calibration.
The membrane that constitutes the sample must be thermalized, to a variable and controlled temperature. Dimensioning of inlet and outlet lines has to take thermal contact and gas accumulation into account.
To maintain the optimal temperature inside the cryostat there are a cold head of a cryocooler, a thermal plate, a thermal shield and copper braids that enable the heat transfer.
During the installation, we put five temperature sensors, see Fig.4.2 and 4.3, respectively:

- in the hp side;
- two sensors on the sample thermalization gauge;
- in the distribution platform;
- on the cryocooler cold head.

In this way, we can control the temperature of the main components of the set-up during the measurements.

Fig. 4.2 – Pictures of the inside of the cryostat, showing:
Left) thermalized sample (Cu ring), middle) thermal shield with Multi-Layer Insulation (MLI) cover, right) closed vacuum vessel.

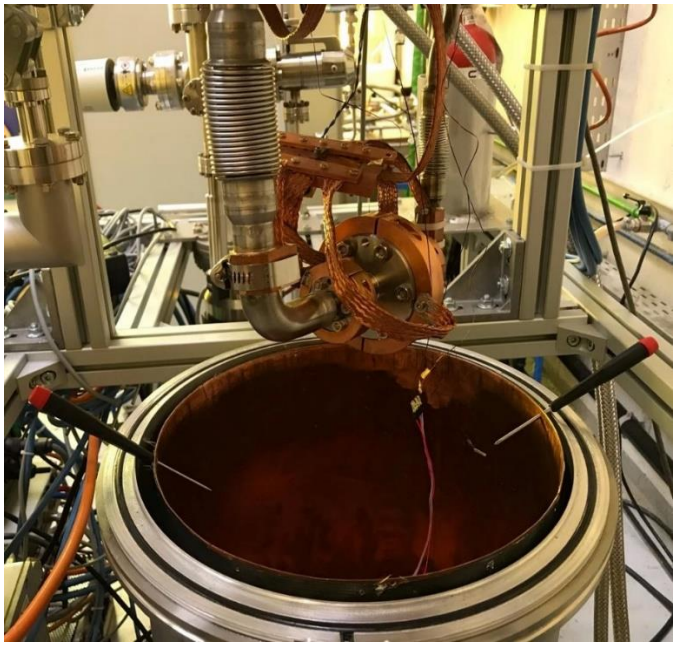

Fig. 4.3 – Picture of the sample and its thermalization connections.

Considering the heat load and the thermal conductance, the lowest temperature reached by the system158 is about 142 K.

Fig. 4.4 – View of the whole system in the cryolab building.

4.2. Samples

For the measurements, we used polymeric films fitted in DN40 copper gaskets and installed between two standard DN40 conflated flanges, as it is shown in Fig. 4.5.

Fig. 4.5 – Polymeric samples used for the measurements.

In particular, the samples are spiral made and realized with DuPont Kapton HN; they diversify themselves for the realization: following Fig. 4.5, the first sample to the left is made by four layers of DuPont Kapton HN with different thicknesses, 12.7 μm, 50.8 μm and two in 125.4 μm, respectively. During its realization, on each layer a coat of 8.7 μm thick glue was put, reaching a total thickness of 140 μm. Finally it present an overlap between the layers of 10 mm. The other two samples are made by three layers, two tapes in 12.7 μm and one in 127 μm; also in this case, a layer of 8.7 μm glue was placed on each tape, reaching a total thickness of 145 μm. The difference between these two samples is that the third one present a significant overlap of 5 mm, as we can see in Fig. 4.6.

Fig. 4.6 – Representation of the two configurations of the second and third samples, respectively.

Anyway the local change of the thickness has been neglected using the nominal thickness for the data processing. Kapton HN polyimide film is a tough, aromatic polyimide film, exhibiting an excellent balance of physical, chemical and electrical properties over a wide temperature range, as low as -269°C and as high as 400°C [31]. The procedure to create these samples is the following one: we have coils made of films of different material. Then we give a spiral shape to these films and thank to a spindle we obtain 6 m tubes: every tube during the coiling is sticked with some special glues. After three days, when the glue evaporates, one can proceed cutting the tubes in the requested samples. Although the sample diameter is 0.040 m we have to consider a smaller diameter during the measurements because the sample is closed in two copper gasket that reduces the free path of the gas to a diameter of 0.0366 m.

4.3. Permeation measurements

4.3.1. Accumulation Method

With this procedure one can measure the permeation rate through the sample.
After pumping high vacuum in the HP and LP sides of the samples, one injects gas in the HP side monitoring it by the PT sensor (see Fig. 4.1). Once the desired value of gas is adjusted, one closes valves V11 and V20. The data recording starts with the moment the sample is exposed to the gas. In this way, gas will permeate from the HP side to the LP ones only through the sample and it will be measured by the capacity sensor CP20.
An example of an accumulation plot is shown in Fig. 4.7, where the horizontal line in the beginning is due to the first phase of gas diffusion into and inside the sample and it is called 'Delay Time'.

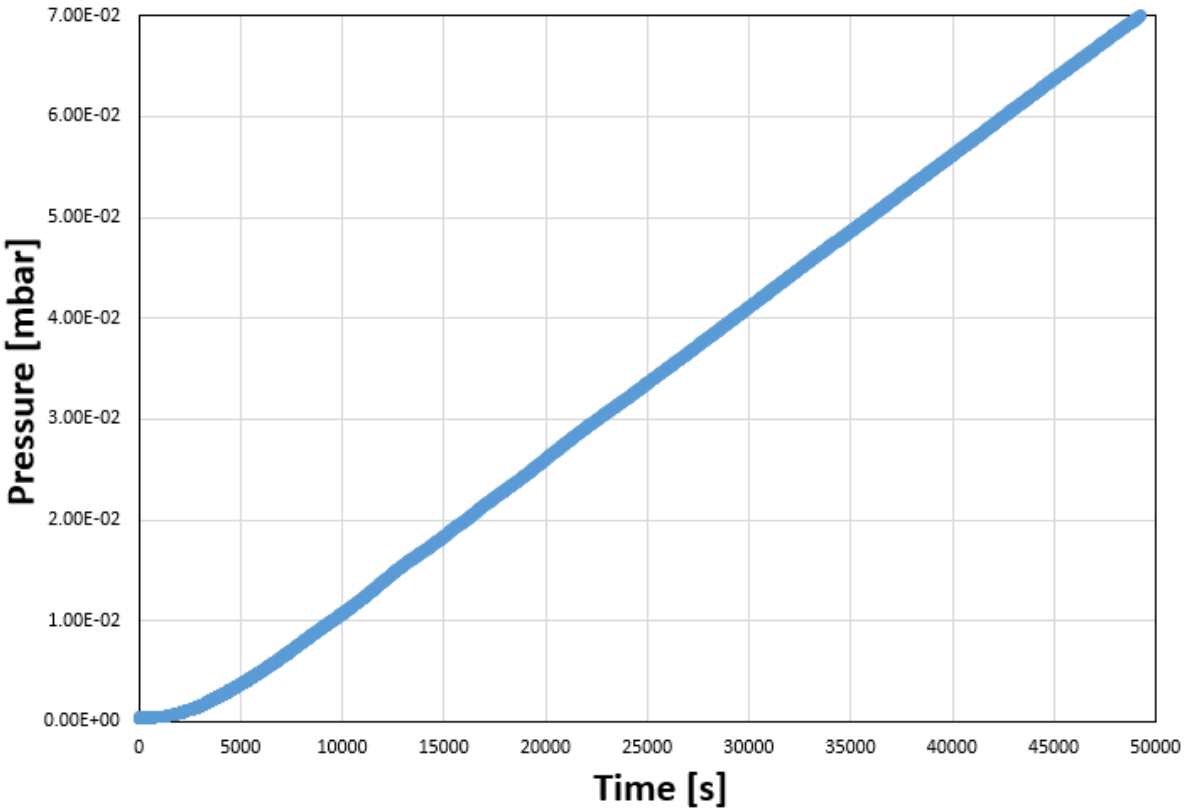

Fig. 4.7 – Trend line of accumulation measured by the capacity sensor.

From this plot, it is possible to calculate the slope dp/dt; then, combining these two equations (4.1) and (4.2) of the flux through the sample with the cross section *A*, thickness *s* and with the LP accumulation volume *V*:

$$\Phi = \frac{p_{hp} * A}{s} * K \quad \left[\frac{bar * l}{s}\right], \tag{4.1}$$

$$\Phi = \frac{dp}{dt} * V \quad \left[\frac{bar * l}{s}\right], \tag{4.2}$$

one can obtain the value of permeated gas, from the following equation (4.3):

$$K = \frac{dp}{dt} * \frac{V*s}{p_{hp}*A} \quad \left[\frac{l}{m*s}\right]. \tag{4.3}$$

One calculates *K* of hydrogen and helium at different temperatures, in order to evaluate the influence of the gas specimen and its temperature dependent permeation.
An example of a permeation measurement result at different temperatures is shown in Fig. 4.8:

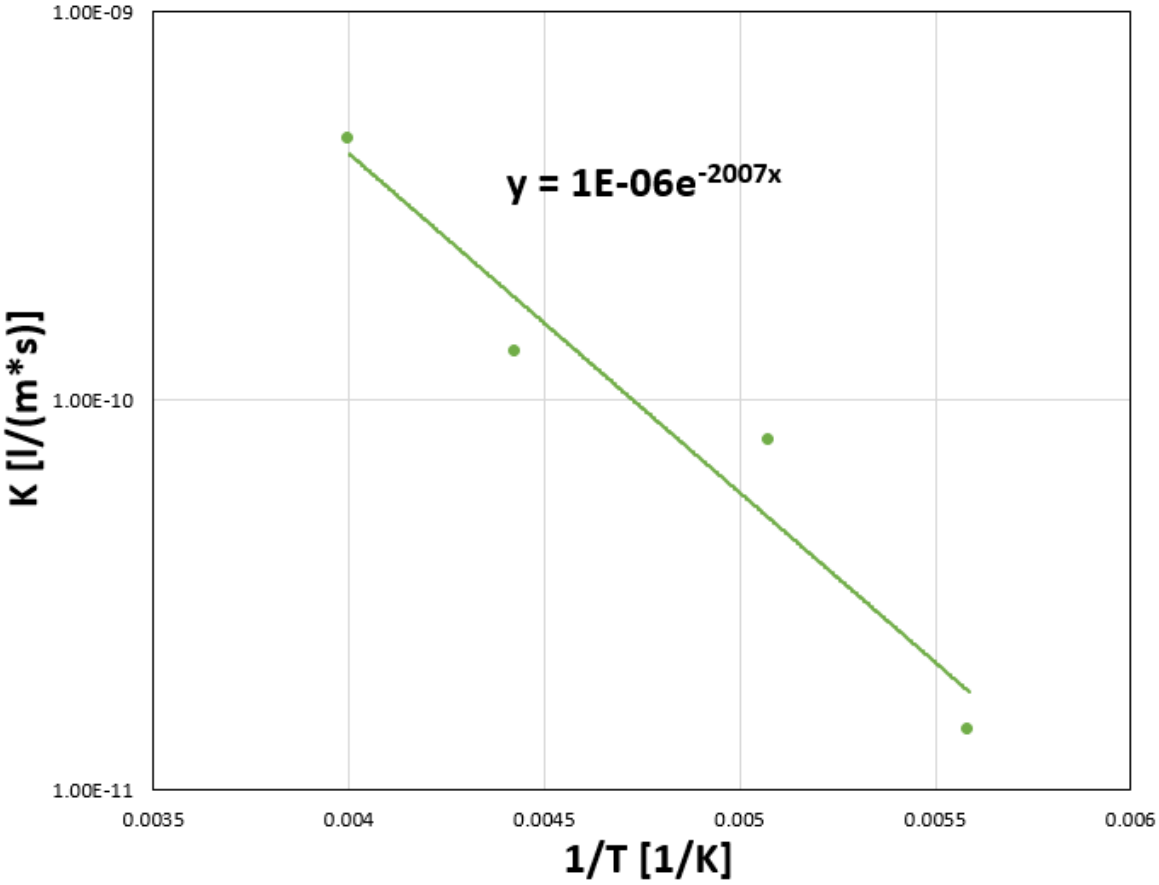

Fig. 4.8 – Helium permeability plotted versus the inverse of temperature.

From the slope of the permeation line in the plot, one can also calculate the activation energy of permeation E_k, following the Arrhenius equation (3.8) that is reported here:

$$K = K_0 e^{\frac{-E_k}{RT}} . \tag{4.4}$$

4.3.2. Residual Gas Analyser

A Residual Gas Analyser (RGA) is a mass spectrometer that measure the chemical composition of a gas and in our set-up is present at the low-pressure side of the sample. Its aim is firstly to ionize separate components of the gas to create various ions and then to detect and determine the mass-to-charge ratios.
It works in vacuum, where the electrically charged beam is propagating with drastically reduced disturbance due to impurities and inconsistencies better detected at low pressure.
In particular, an RGA allows:

- to analyse the various gas phase reactions;
- to monitor the changes occurring in any gas environment;
- to check vacuum leaks;
- to check the mass flow controller, etc.

It is constituted by five main components:

- *Ionizer*, where the neutral gas atoms or molecules are converted into positive ions; it consists of two filaments for producing electrons, an electrostatic wire mesh for setting up a constant electrostatic potential inside the ionization region and insulating holders.
- *Electrostatic lens*, it focuses and accelerates the positive ions into a beam that has about 10-20 eV of energy through a series of electrostatic "lenses".
- *Mass Analyser and Filter*, where accelerated and focused positive ions are sorted put according to their respective masses by employing electric and magnetic fields; this unit acts as a filter, it filters the ions with mass-to-charge ratio chosen by the user while all the other ions get deflected aside into the walls where they neutralize and become undetectable.
- *Ion Detector*, which detects and calculates the mass-to-charge ratio of the filtered ions as ion current with an extended secondary electron multiplier. Choosing a specific mass-to-charge ratio and making a measurement of the signal obtained, it is possible to figure out the number of those molecules present in the ionizer region of the RGA.
  Passing through a whole range of M/e ratios, one can find a whole range of molecules that are present and begin to understand the full range of chemical components in the gas.
- *Mass Spectrum*, which depicts peaks of ions with mass-to-charge ratios in "a.m.u.-atomic mass unit" which corresponds to the mass of one proton.
  These M/e are characteristic of all elements: peaks in the spectrum of 2 a.m.u. is H_2, 4 a.m.u. is He, 14 a.m.u. is N, 18 a.m.u. is H_2O 28 a.m.u. is N_2, etc. An example of mass spectrum is shown in Fig. 4.9: in our measurements, we read the sprectrum until around 50 a.m.u. because the elements after that value are all heavy hydrocarbons and those are not present in our set-up.

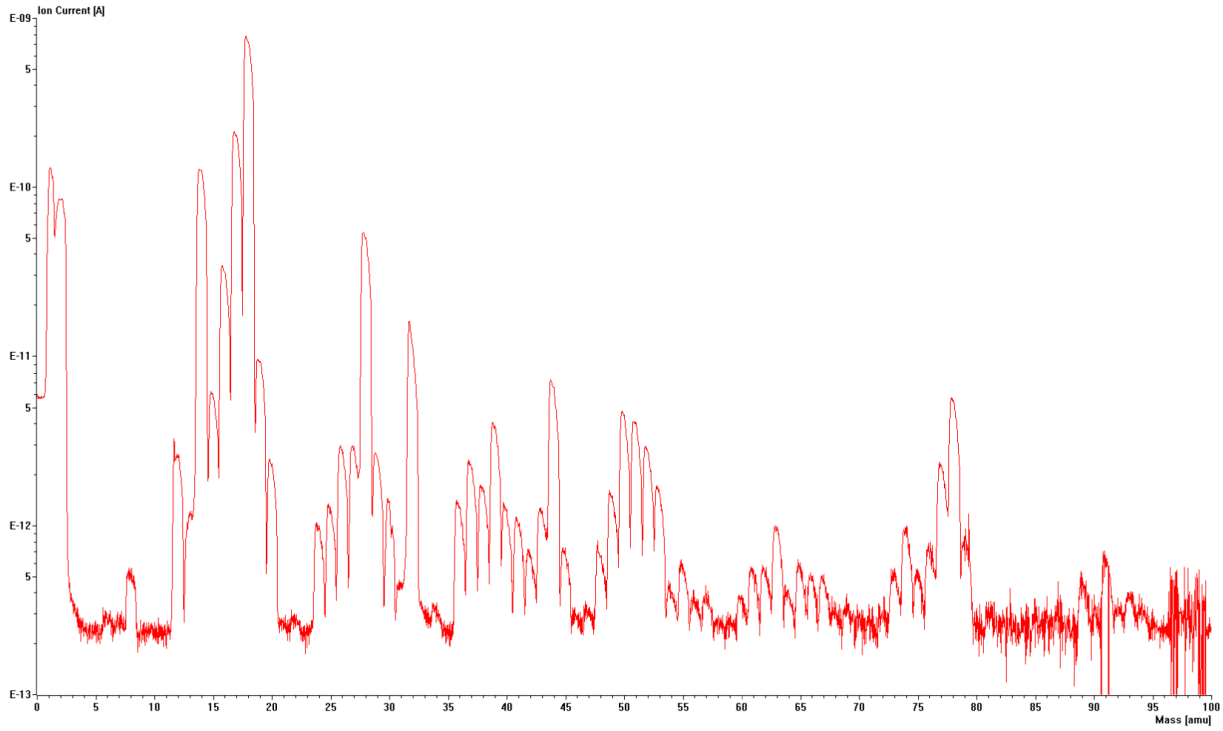

Fig. 4.9 – Spectrum generated by an RGA.

4.3.2.1. RGA calibration for Hydrogen

The first step to start using the system is the RGA calibration, which consists of calibrating the RGA signal in [A] with the pressure signal, read by the penning gauge in mbar (see Fig. 4.10).
We inject gas in the system until it permeates in the LP side through the sample. Valve V20 is opened gradually and, when the flux is stable, data from penning gauge, full range and RGA are recorded. The calibration finishes when a sufficient amount of measurement data is collected; the noise of both gauges must be subtracted from the measures.
The penning gauge reads the pressure in nitrogen equivalent pressure: all pressures read by the penning gauge need to be multiplied by the respective ionization factor (see Tab. 4.1), in order to transform those data in helium or hydrogen equivalent pressure.

Tab. 4.1 – Ionization factor for some gases [18].

Gas	Factor
Air	1.02
Xe	0.41
Kr	0.59
Ar	0.85
H2	2.49
Ne	4.55
He	7.24

For the measurements, it is also necessary to know the pumping speed of the turbo-molecular pump in the LP side, described in Tab. 4.2; it is installed directly in the system, so no-conductance has been considered for the measurements.

Tab. 4.2 – Pumping speed of the turbo-molecular pump in LP side.

Gas	Pumping speed [l/s]
Air	210
Hydrogen	220
Helium	180

If the penning gauge works well, the data set constitutes a straight line and its slope is the calibration coefficient (see Tab. 4.3 and Fig. 4.10).

Tab. 4.3 – Hydrogen data from RGA calibration.

$p_{penning}$ gauge [mbar]	Ion Current [A]
2.00E-09	2.73E-12
8.70E-09	1.08E-11
1.90E-08	2.63E-11
5.10E-08	7.42E-11
9.20E-08	1.34E-10
2.00E-07	2.92E-10

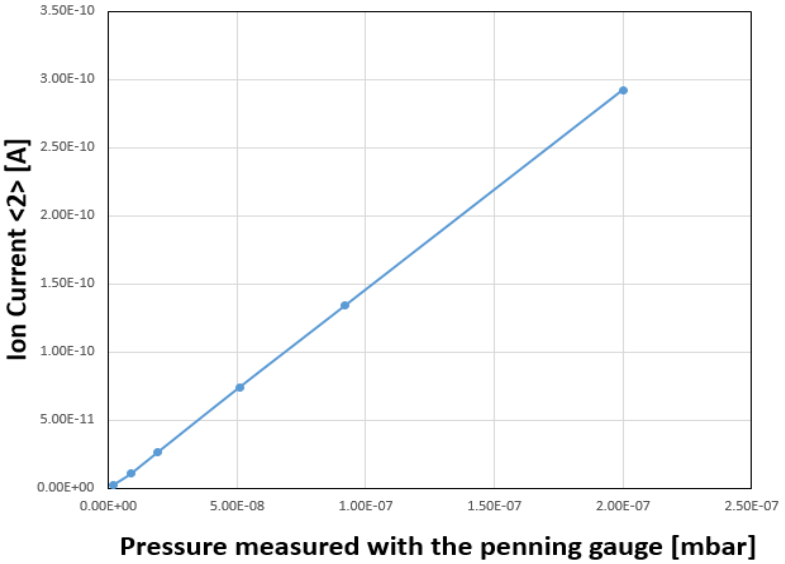

Fig. 4.10 – RGA calibration line for hydrogen.

4.3.2.2. RGA calibration for helium

In this case, we used a helium calibrated leak, mounted on the LP side. The calibrated leak, shown in Fig. 4.11 has a flux of 1.7×10^{-7} mbar l s^{-1}.

Fig. 4.11 – Helium calibrated leak mounted on LP side of the system.

In case of helium, the calibration coefficient is given by the equation (4.5):

$$r = \frac{I_{Cl} S_{eff}}{J_{Cl}}, \tag{4.5}$$

where J_{Cl} e I_{Cl} are the calibrated leak flow and current signal read by the RGA, respectively.

4.3.3. Integration Method

After gas has been accumulated with the valves V11 and V20 closed, one opens the valve V20: gas is slowly released in the LP side, monitored by the RGA. The area of the experimental curve given by the integration of the RGA signal over time is directly proportional to the quantity of accumulated gas.
The measurement ends when the RGA curve becomes flat again and with values equal to the initial ones.

We use this integration method for both helium and hydrogen measurements.

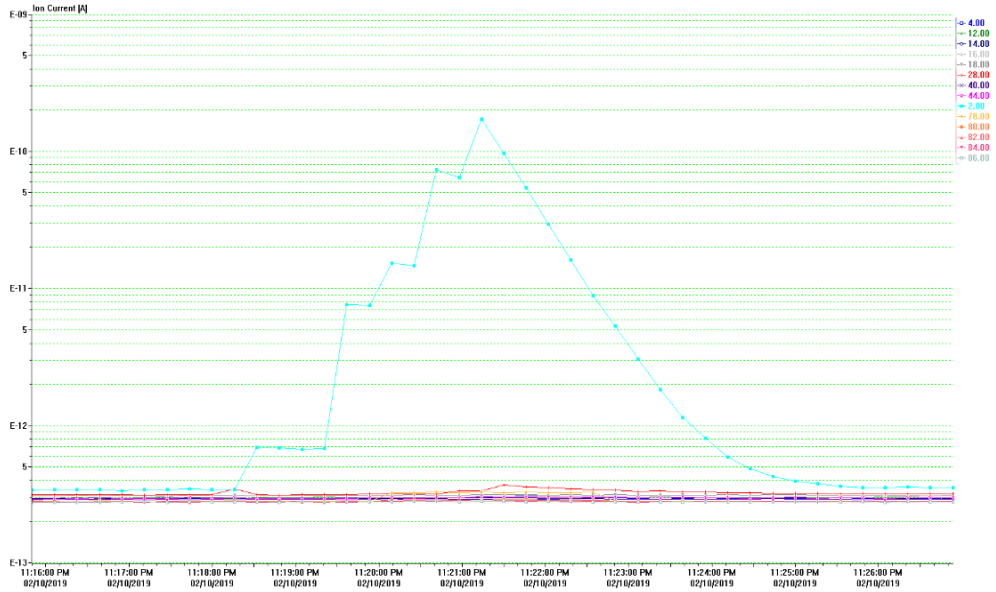

Fig. 4.12 – Detection of the mass-to-charge ratio of the hydrogen filtered ions as ion current versus time by the RGA for the integrated method.

As we can see in Fig. 4.12 every gas is presented with a different colour, in particular I chose hydrogen in light blue while helium in blue. From this type of plot and then method one can evaluate if the measure is clean or not: the measurement of hydrogen shown in Fig. 4.12 is distinctly clean because what is increased is only hydrogen while the other gases proceeded without increasing and in a negligible way. Sometimes it happens that when one measures helium one finds hydrogen that was entrapped inside the sample from the previous measurement also after having purged the chambers (see Fig. 4.13), or other gases like water vapour, oxygen and other components of air that increase during the measurement (see Fig. 4.14): this means that inside the chambers water or air is accumulated during the purging at room temperature.

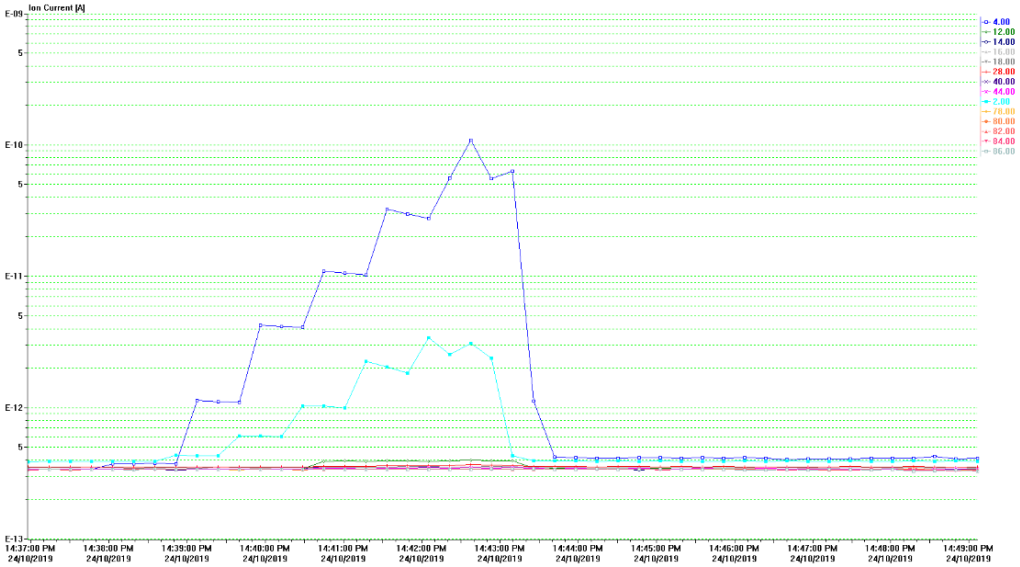

Fig. 4.13 – Plot of helium integration method with traces of hydrogen.

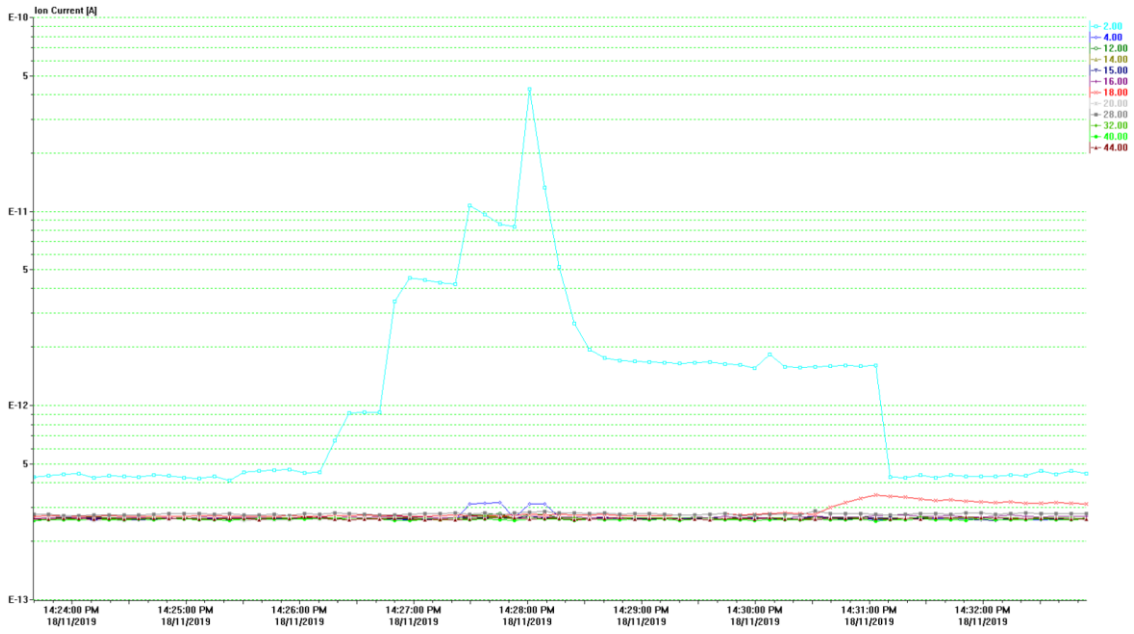

Fig. 4.14 – Example of hydrogen integration method with traces of helium and vapour water.

Then, we calculate the ratio dp/dI from the following plot in Fig. 4.15, in which it is represented the ion current as a function of pressure measured both with the full range and penning gauges, downstream of the LP side:

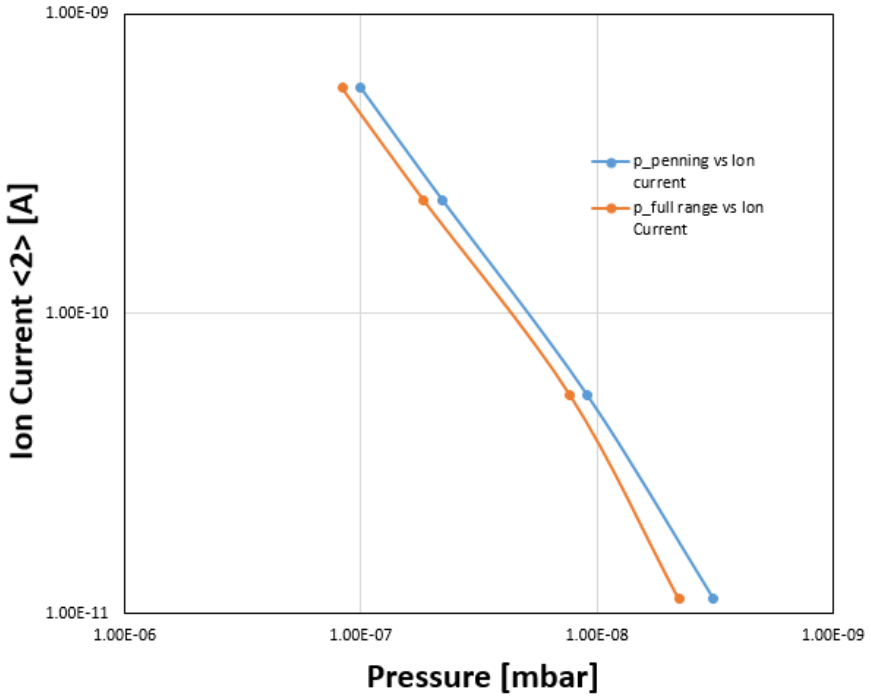

Fig. 4.15 – Trend of current of the RGA as function of both full range and penning gauges.

In this way, one can get the flow rate of permeated gas and we can compare it with that one found with the accumulation method. The flow rate equation used with this method is explained in the equation (4.6):

$$\Phi = \frac{S}{\Delta t}\frac{dp}{dI}\int Idt \quad \left[\frac{bar*l}{s}\right], \tag{4.6}$$

where S is the pumping speed of turbo-molecular pump in the LP side and it is S = 220 [l/s] for hydrogen and S = 180 [l/s] for helium.

4.4. Diffusion Measurements

As presented in chapter 3, we can estimate the diffusion coefficient D from experimental data by the equation of the 'time constant' (3.24):

$$t = \frac{l^2}{6D}, \tag{3.24}$$

The time constant is the span of time in which the injected gas in the HP side is soluting on the sample surfaces and diffusing through the sample thickness. This time span is shown in Fig. 4.16 as the range delimited by the two red signs:

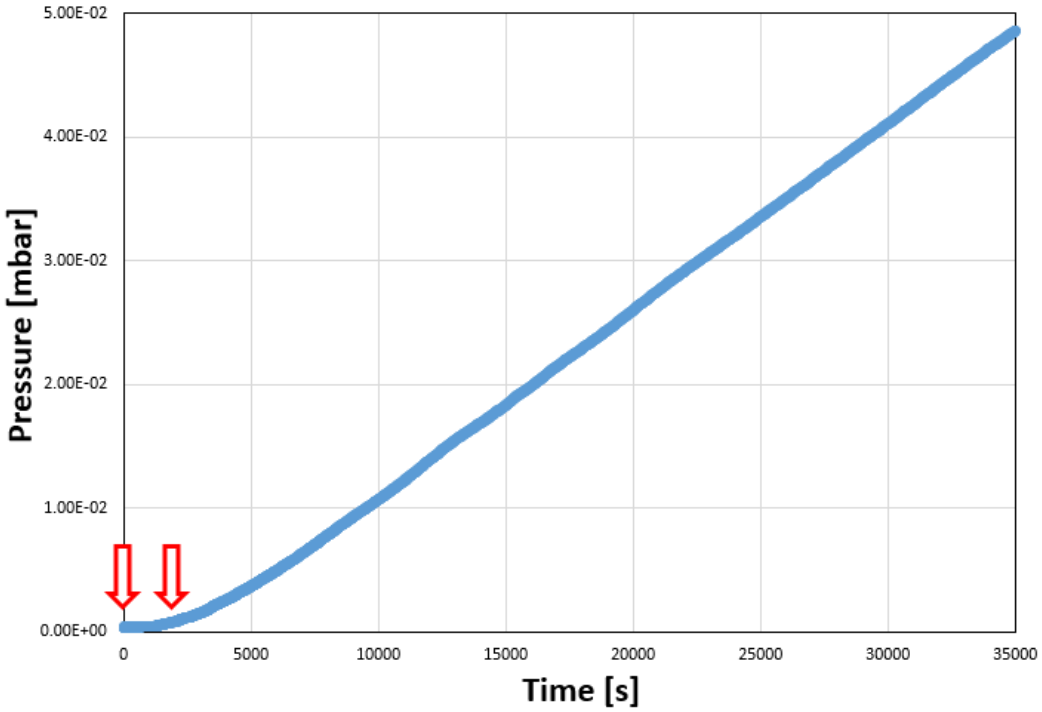

Fig. 4.16 – Trend of diffusion and permeation processes through the sample.

4.5. Solubility Measurements

After we have experimentally measured the permeation and then calculate the diffusivity, we can evaluate also the solubility coefficient by the equation (3.17) that was introduced in chapter 3 and that we report here:

$$K = DS. \tag{3.17}$$

5. Results

After having done all the measurements for the two main gases Hydrogen and Helium and the pre-exposure with Krypton, the results have been obtained.

5.1 Kapton DuPont HN made by four layers

5.1.1 Permeation results

- Hydrogen

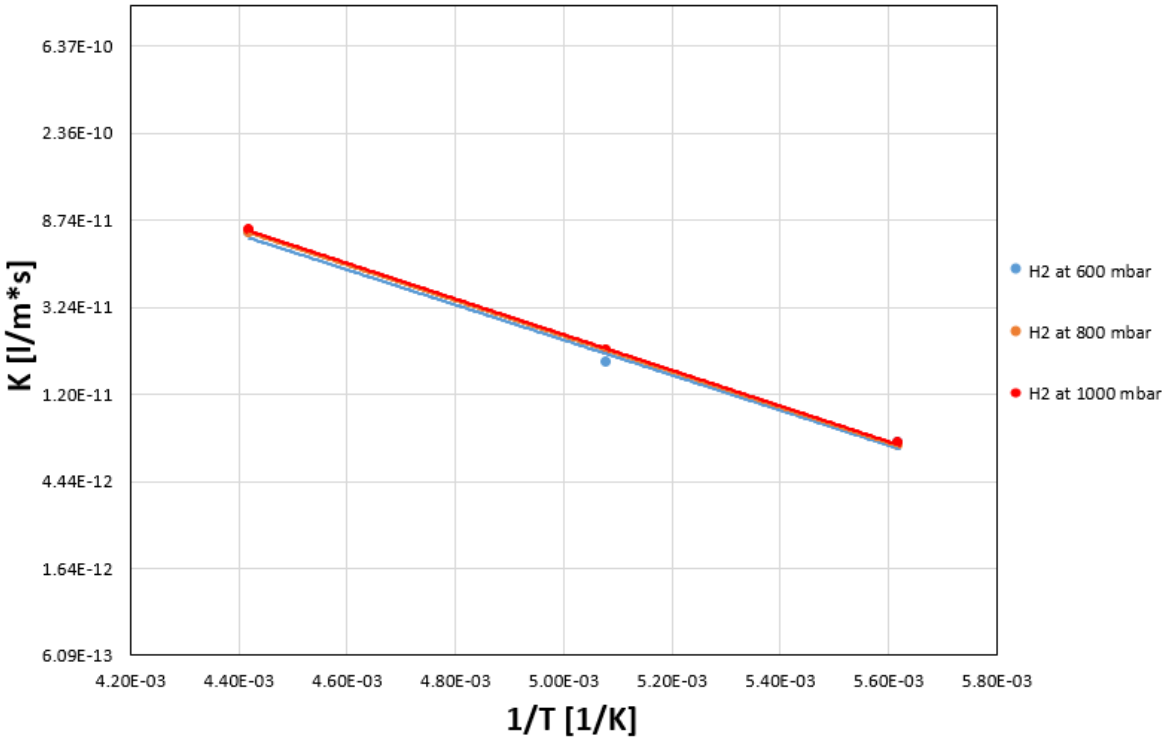

Fig. 5.1 – Plot with all the measurements of hydrogen at different pressures of injection and temperatures.

The plot in Fig. 5.1 shows the coefficient of permeability *K* as function of the inverse of the temperature. The measurements were done at 226 K, 197 K and 178 K, and for each temperature hydrogen has been injected at three different pressure of injection, respectively 600 mbar, 800 mbar and 1000 mbar.
As we can see the lines are parallel to each others and show a decreasing slope, going from the highest temperature to the lowest one, were we reach 9.84E-12 [l/s*m] as minimum of permeation.
This plot also shows that the K parameter is very little influenced from the pressure of injection: passing from 600 mbar to 1000 mbar the values of permeations are quite the same for each temperature.

- Helium

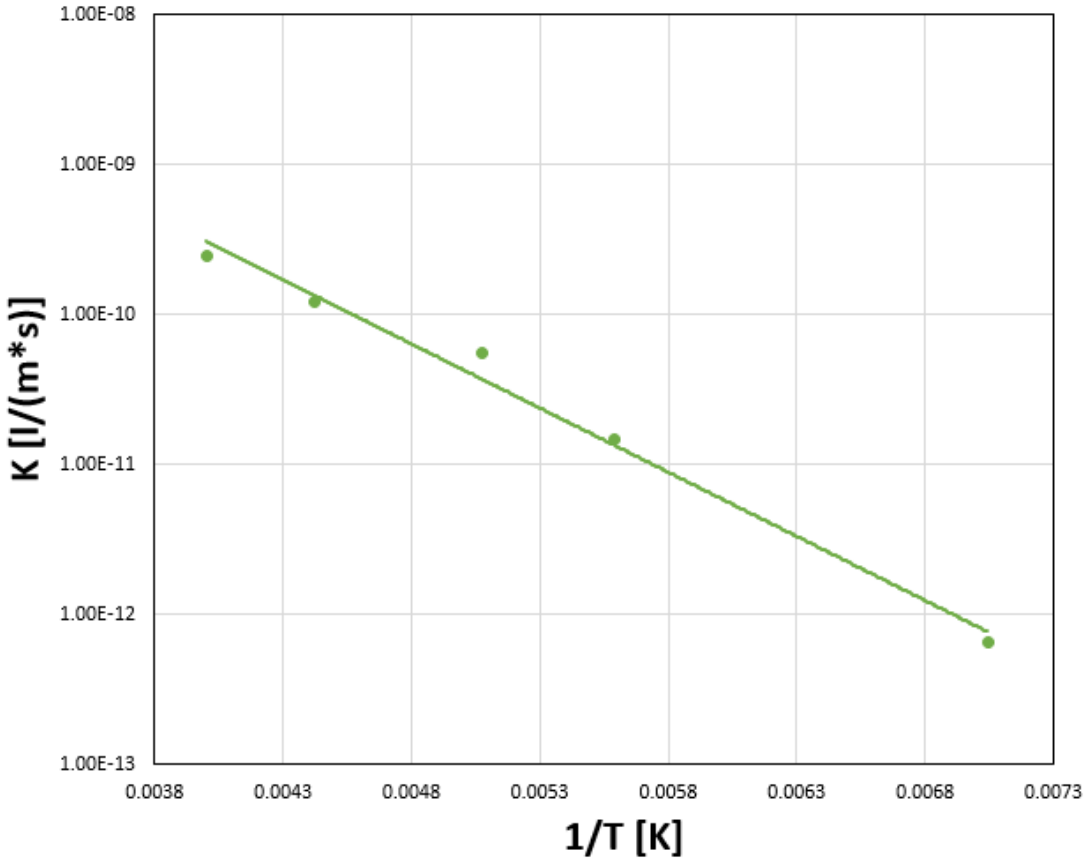

Fig. 5.2 – Plot with all the results of helium at different temperatures with a pressure of injection of 800 mbar.

This plot shows the measurements with helium at five different temperatures, respectively 250K, 226 K, 197K, 178K and 142 K. For each point of temperature, 800 mbar of helium has been injected and the results are shown in Fig. 5.2. As expected the minimum value of the permeability coefficient, around 5.80E-13 [l/(m*s)], is reached at the lowest temperature of 142 K, corresponding to a value of 1/T = 0.007.
In order to reduce the permeability of helium and light gases in general, with this first sample an innovative solution has been tried: it consist in injecting a heavy gas, krypton, at room temperature, cooling down the set- up, purging the chambers and then charge with helium respectively to 142 K, 179 K and 226 K: the result is shown in Fig. 5.3.
Krypton has 84.80 as atomic weight, 21 times bigger than helium that has 4.00 as atomic weight; this means that krypton needs more time to permeate through the sample in comparison to helium and also with more time it is difficult for this heavy gas to find a path through the lattice structure of the sample due to its dimensions.

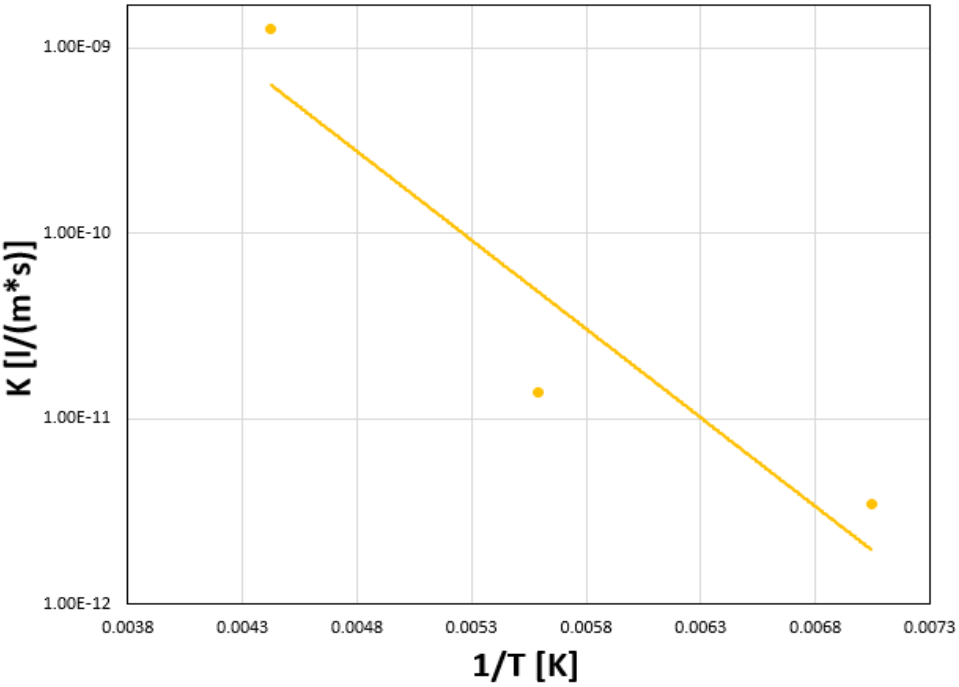

Fig. 5.3 – Plot with helium after krypton.

The aim was to reduce the permeation of helium through the sample saturating it before with krypton: the two lines, one of helium and one of helium after krypton respectively, can be compared in the following Fig. 5.4.

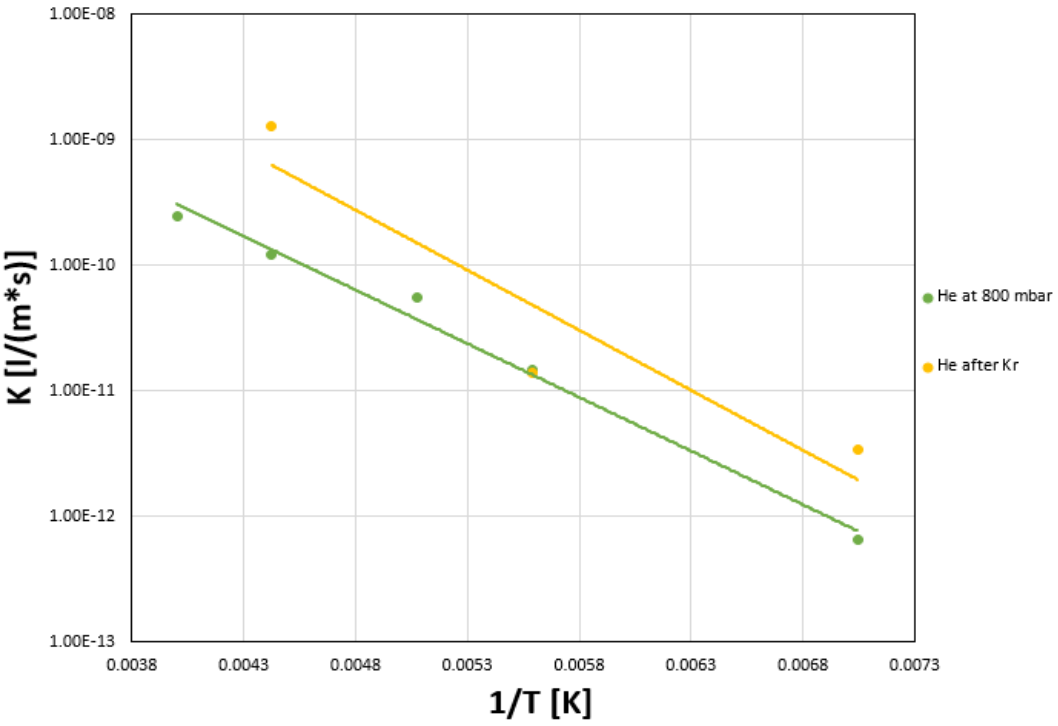

Fig. 5.4 – Comparison between helium and the behaviour of helium after krypton.

Unfortunately, this strategy didn't show the intended effect. Even an increase in helium permeation after krypton exposure is recorded (see Fig. 5.4). So for the next samples this strategy has been abandoned.

- Comparison between hydrogen and helium

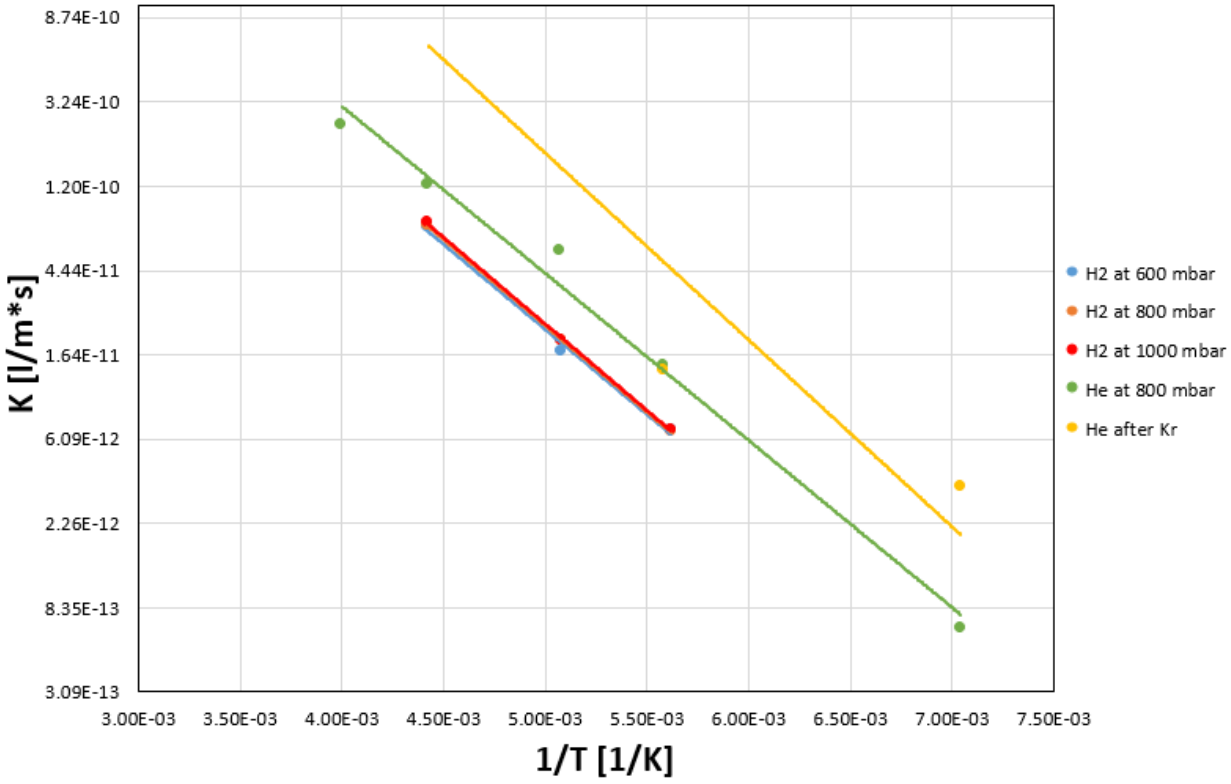

Fig. 5.5 – Plot showing the comparison of all tested gases and the respective test conditions. The three lines of H2 tests are almost overlapping, compare Fig. 5.1.

Finally in Fig. 5.5 all the results of permeation measurements done with the first sample are shown: the plot shows a higher concentration of helium as permeant in comparison to hydrogen also if helium has a bigger atomic weight than the hydrogen. The explanation is that hydrogen is a molecule and therefore occupies a larger volume compared to helium atoms.

5.1.2 Diffusion results

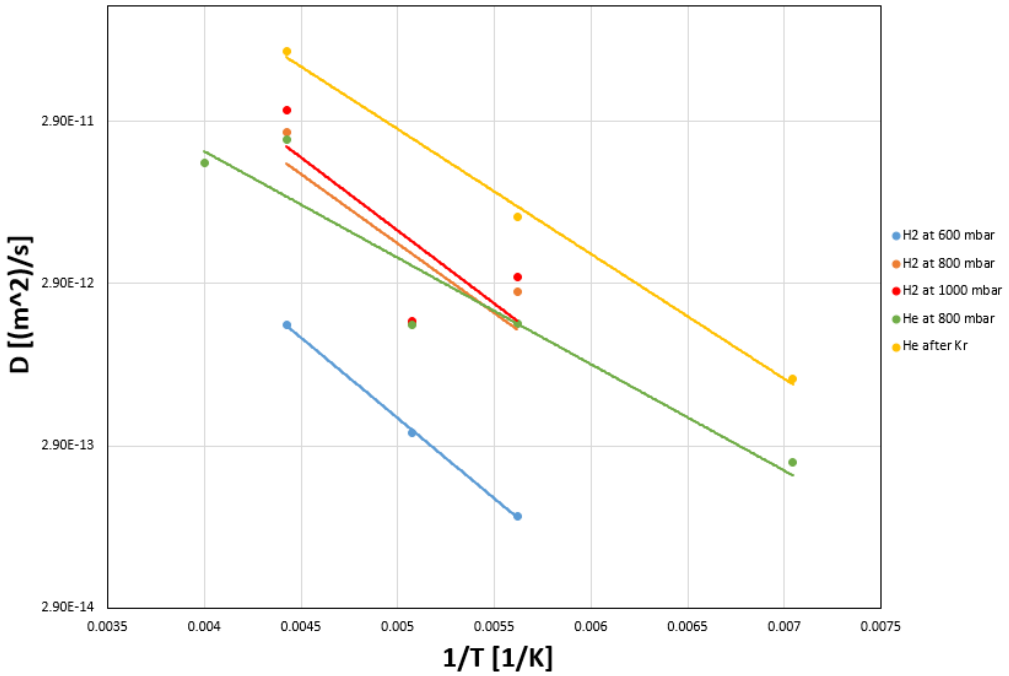

Fig. 5.6 – Comparison between the diffusion results of different gases.

Fig. 5.6 shows a plot with all the measurements in terms of diffusion which are determined. For hydrogen, its injection at 600 mbar of each temperature gives the minimum value of permeation while all the other measures at major pressure of injection are close to each other and an higher value.

5.1.3 Sorption results

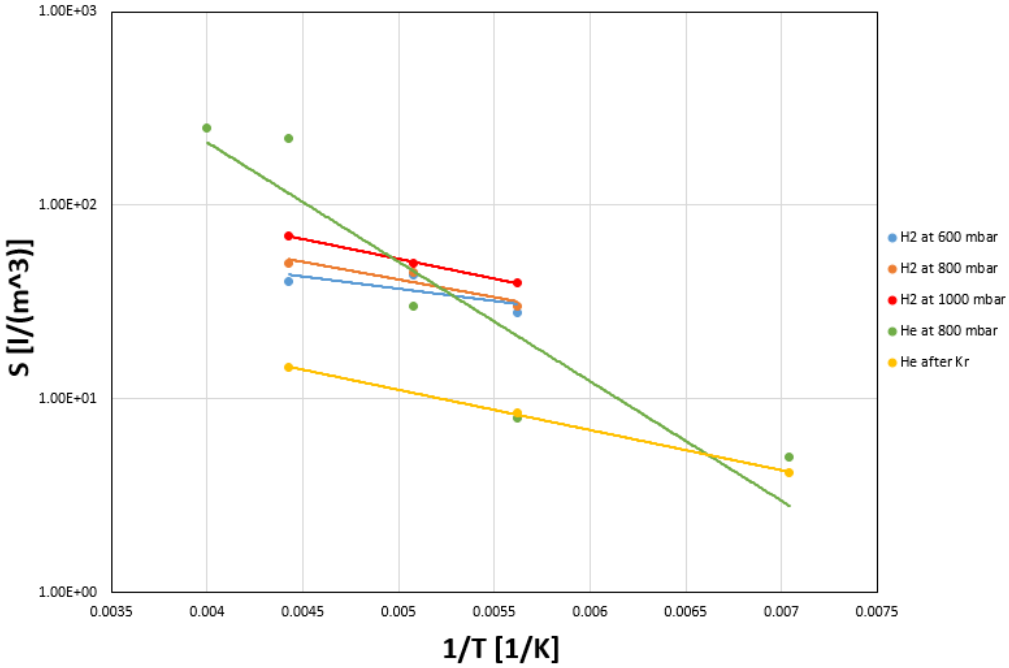

Fig. 5.7 – Comparison between the solubility results of different gases.

Seen the great differences in analysed values of solubility (see Fig. 5.7), pure helium and hydrogen show a very different behaviour in terms of temperature dependence (slope in the graph), with a high solubility of He at higher temperatures. This behaviour seem to change when the sample was pre-exposed with krypton. The slope of the helium approached the one of hydrogen but with much bigger values. This can lead to the statement that the krypton actually triggers the solubility of helium at the surface and in the material and by that may also trigger the higher diffusivity values that we have observed.
The overall process with pre-exposure of a heavy noble gas seems to be more complex than in the initial idea for the study.

5.2 Kapton DuPont HN made by three layers, without overlap

5.2.1 Permeation results

- Hydrogen

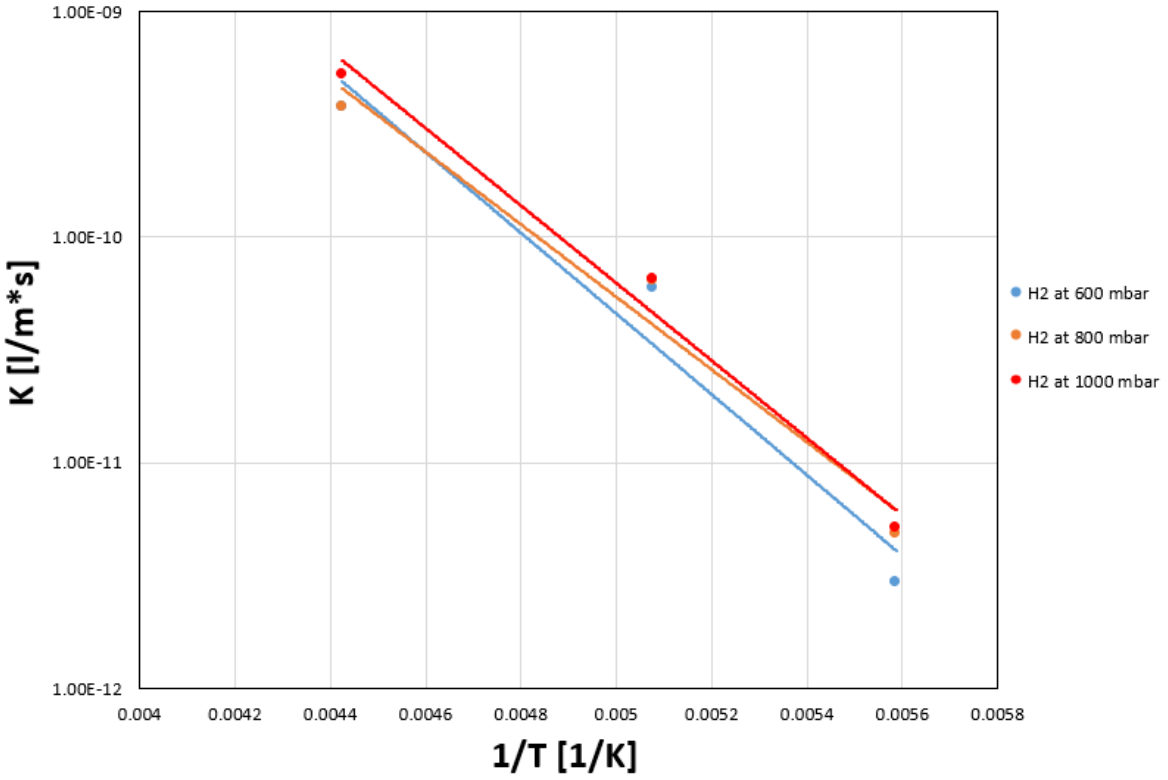

Fig. 5.8 – Plot with all the measurements of hydrogen at different pressures of injection and temperatures.

In Fig. 5.8 the measurements with hydrogen with the second sample are reported. For a better understanding and comparison, the measurements has been done at the same temperatures which were used with the previous sample, 179 K, 197 K and 226 K respectively. In this case, the same rate of permeation was reached in less time than the first sample, suggesting a worse behaviour for the second sample made with the same material but realized with three different layers and without overlap.

- Helium

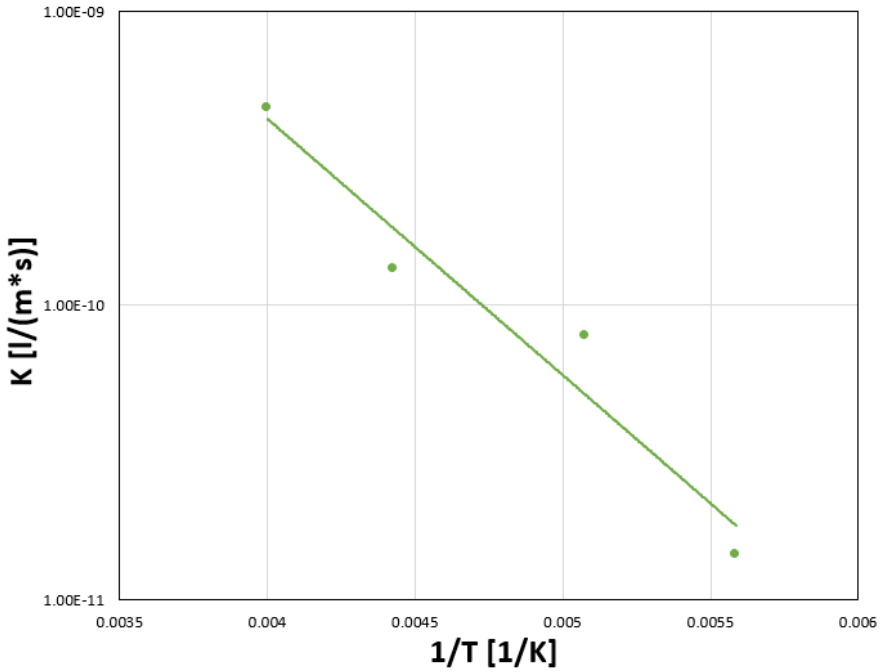

Fig. 5.9 – Plot with all the measurements of helium at 800 mbar as pressure of injection and different temperatures.

The plot in Fig. 5.9 shows the permeability results of Kapton DuPont injecting helium. The measurements has been done injecting helium at a constant pressure of 800 mbar for each temperature, 179 K, 197 K, 226 K and 250 K, respectively. As for the previous sample, the first temperature with which the helium measure has been performed was 142 K but it led to an unexpected result (see Fig. 5.10):

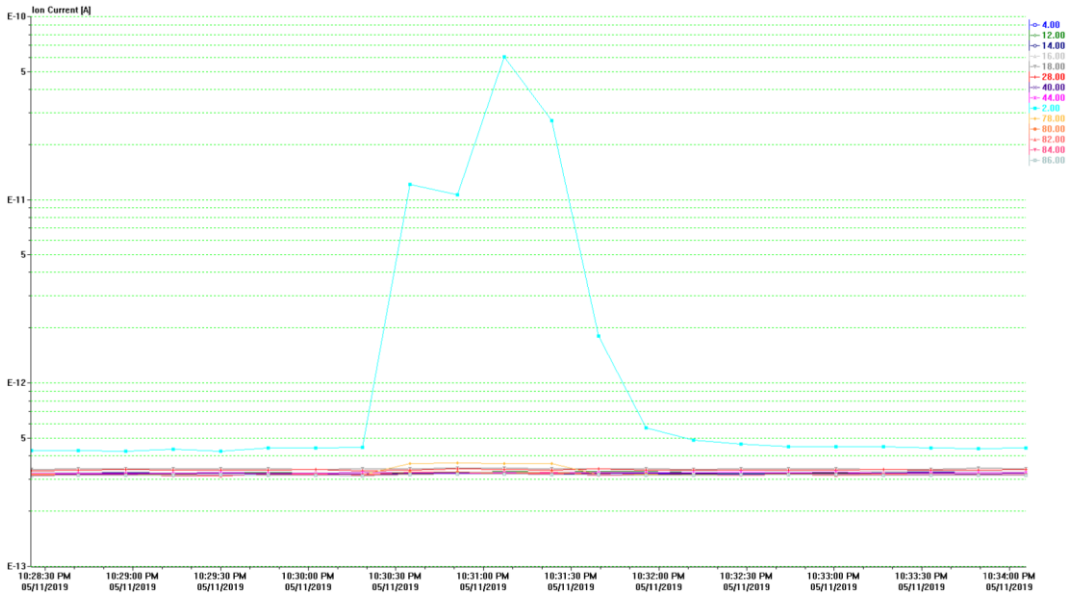

Fig. 5.10 – Plot representing the helium measure done at 142 K with the integration method: only hydrogen is permeated.

From the results of the dynamic measurement carried out with the integration method, we see that the sample remained saturated with hydrogen despite the chambers have been cleaned from the previous measurement with hydrogen and helium didn't pass at all. The measurement has been carried out twice and it has led to the same result.

5.2.2 Diffusion results

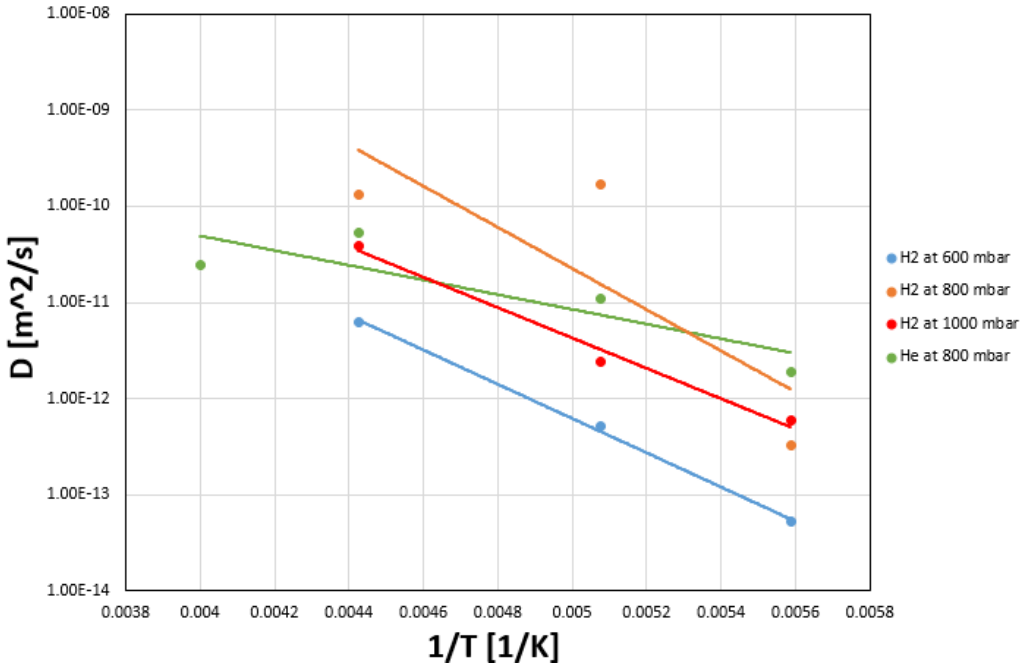

Fig. 5.11 – Comparison between the diffusion results of different gases.

5.2.3 Sorption results

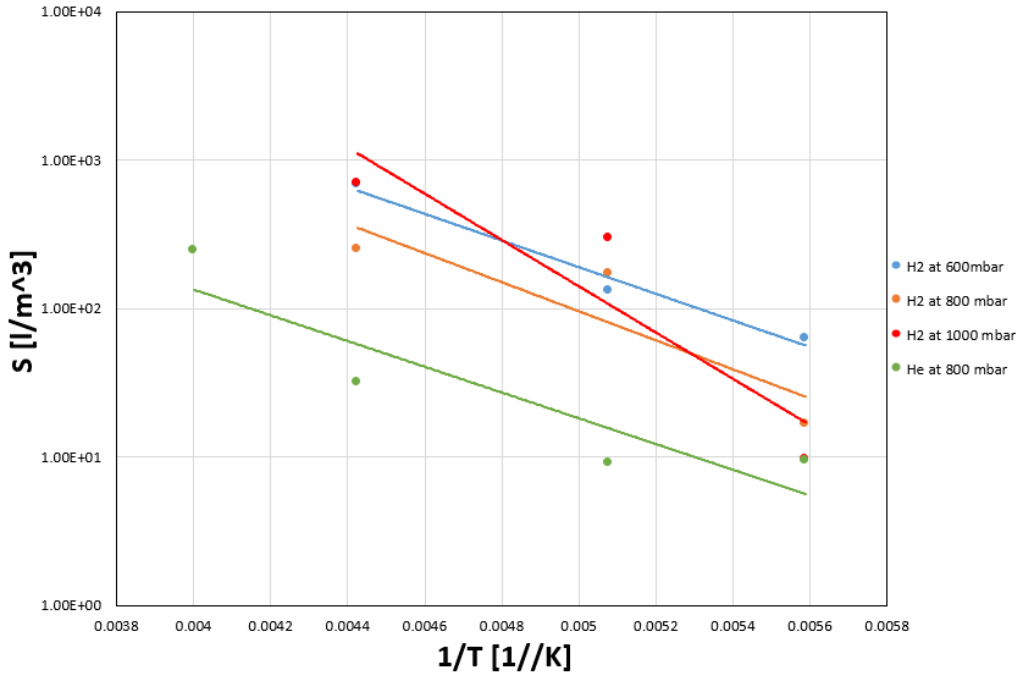

Fig. 5.12 – Comparison between the solution results of different gases.

5.3 Kapton DuPont HN made by with overlap

With this last sample there were some problems during the measurements, due to the configuration of the sample itself. In fact, it is the only one that presents an overlap exposed to permeation, close to the copper gasket; this leads to having a different thickness along the junction between the part with the overlap and that without, causing a leak during the measurements. For this reason, the measurements at 600 mbar and 800 mbar did not lead to any result, as the little gas that permeated escaped from the leak and did not accumulate in the chamber downstream the sample. We then proceeded by making a single measurement for each temperature at a higher injection pressure of 1000 mbar, for both hydrogen and helium, keeping the V11 open and thus ensuring a continuous and constant injection pressure.

5.3.1 Permeation results

- Hydrogen

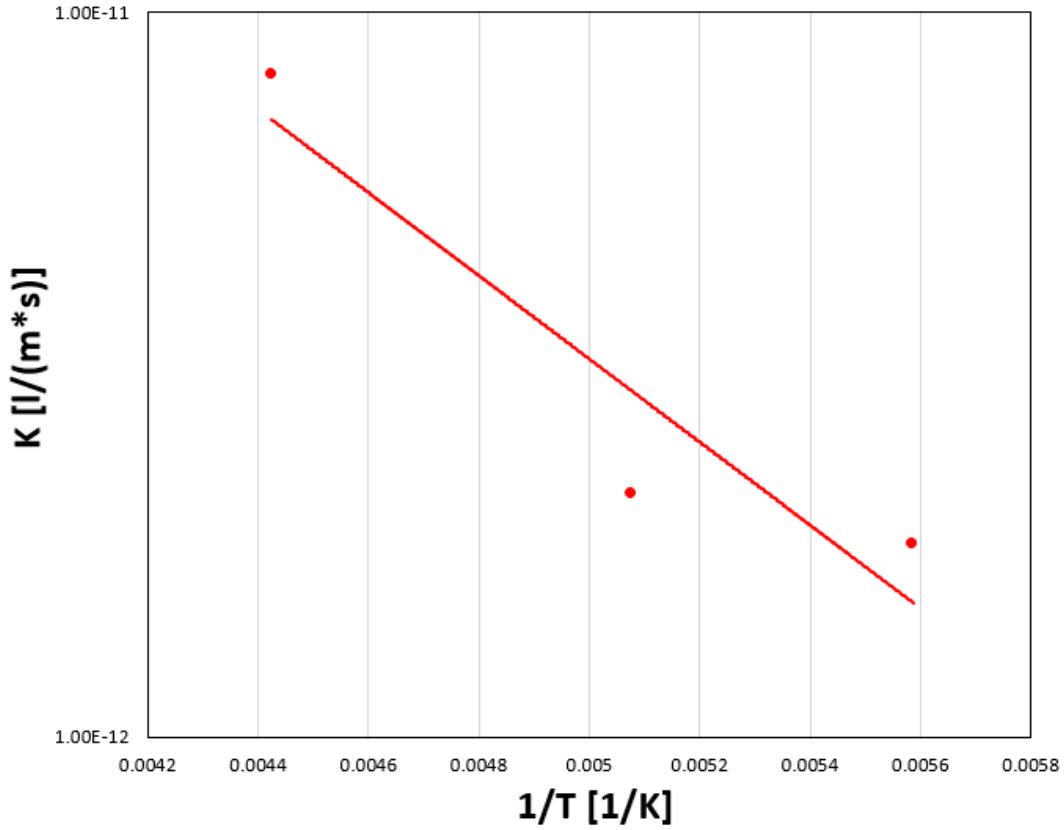

Fig. 5.13 – Representation of hydrogen permeation measurements with 1000 mbar as pressure of injection and at different temperatures.

In Fig. 5.13, the three hydrogen measurements are collected: as it is written above, we did one measure for each of the three level of temperature, 179 K, 197 K and 226 K respectively. With this plot we can estimate a permeation value of 1.84E-12 mbar for the lower temperature measured, and a good decreasing trend of permeation going from left to right of the plot.

- Helium

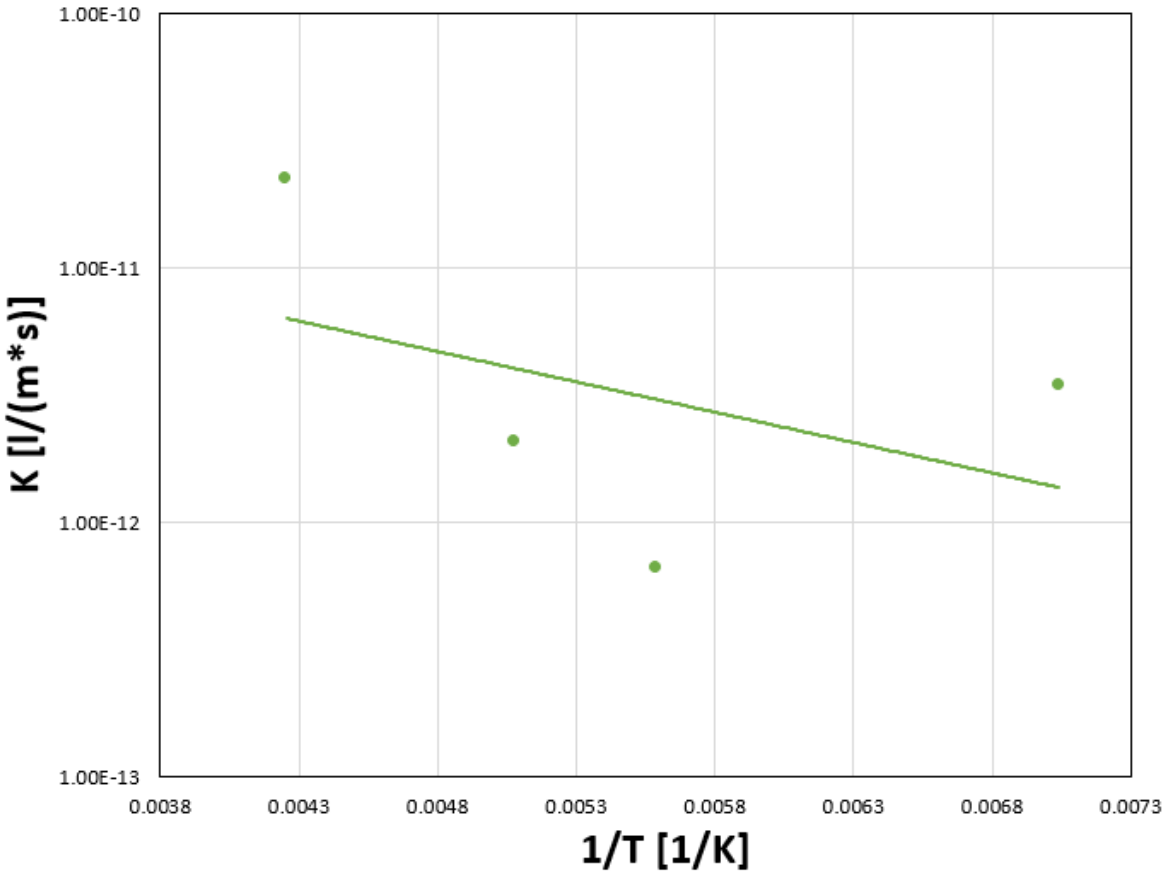

Fig. 5.14 – Representation of helium permeation measurements with 1 bar as pressure of injection and at different temperatures.

For helium, as we can see in Fig. 5.14, we collected one measure for the following temperatures: 142 K, 179 K, 197 K and 235 K; respect to the other samples, we tried a measure considering an average between the temperatures 226 K and 250 K because the thermal plate didn't manage to reach 250 K as the previous times.
The points collected are close to each others, showing a flatter permeation tendency: this lead to have a higher permeation coefficient at the lower temperatures respect to the other samples. We can state that for helium as a permeant, this sample shows inconclusive results, probably generated due to the overlapping sample structure and the mentioned small leaks that may vary the overall sample behaviour not to be pure diffusion like.

5.3.2 Diffusion results

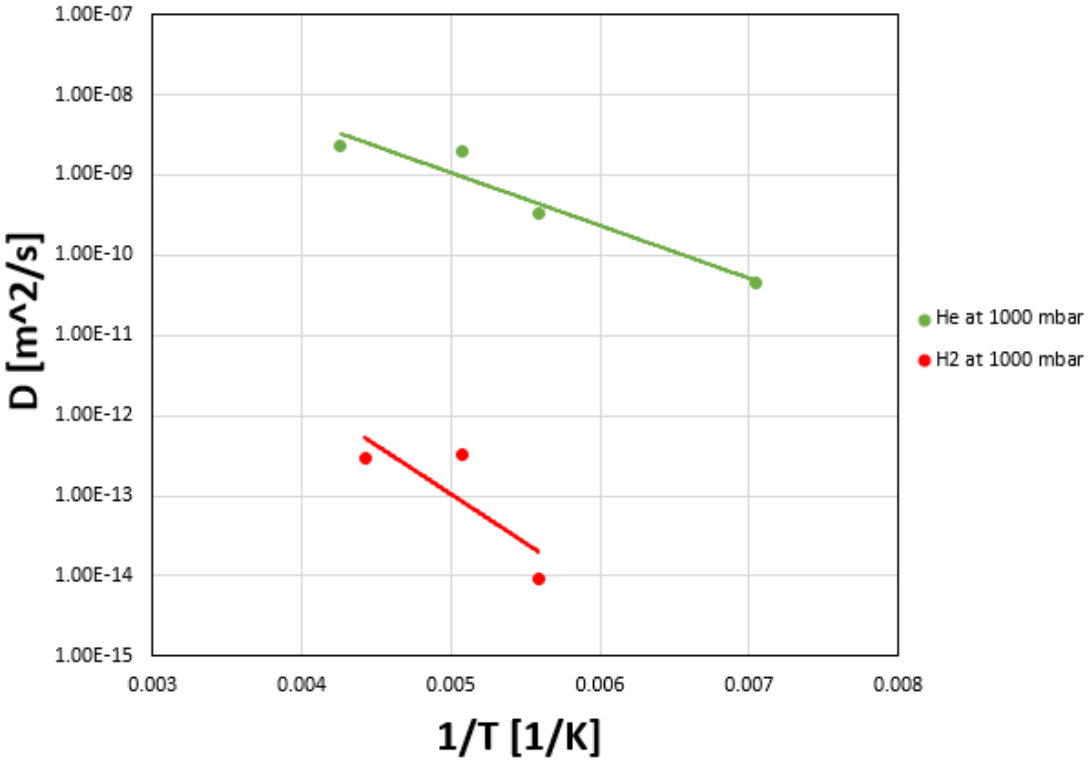

Fig. 5.15 – Representation of hydrogen and helium diffusion measurements with 1 bar as pressure of injection and at different temperatures.

5.3.3 Sorption results

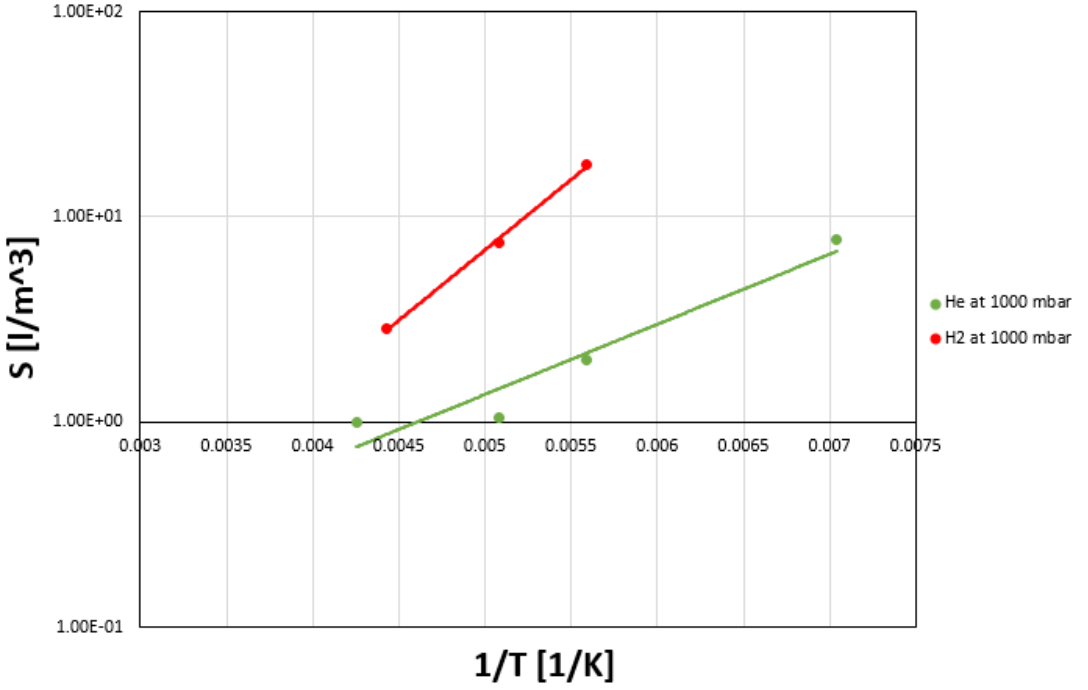

Fig. 5.16 – Representation of hydrogen sorption measurements with 1 bar as pressure of injection and at different temperatures.

Conclusions

Polymers have a good application in the field of low-temperature UHV as shown by their use in terms of target and detectors for the accelerator experiments. The COMPASS experiment has given the opportunity to study polymeric barrier properties at very low temperature increasing our knowledge about these materials.

Measurements have been performed with three samples made by Kapton DuPont HN with three different configurations, for a range of temperatures between 142 K and 250 K with hydrogen and helium as permeant gases. The strategy of injecting a heavy gas, krypton in this case, to saturate the sample, clean the channels around the sample and proceed with standard measurements was abandoned after testing it in the first sample: in the time frame set for the measurement, the Krypton was not able to saturate the sample, as in the following measure the helium had no difficulty in permeating the sample.

Thanks to the Arrhenius equation it is possible to estimate the temperature dependence of the permeation from the results acquired. Furthermore, activation energies for permeation and diffusion have been calculated for all the polymers, such as the flux of injected gases through the samples with both the static and the integrated methods. Since the helium has a smaller size than the hydrogen molecule, helium has shown a bigger permeation and diffusion than hydrogen in the three samples. All the results are summarized in the tables in the Appendix A.

Comparing the results of the three samples and calculating the permeation values for each sample at the COMPASS work temperature, the best candidate seems to be the second sample, made by three layers with different thicknesses in Kapton DuPont HN.

The measurements on the third sample show interesting results in terms of permeation; however, considering the leak present in the sample, these results are not very reliable.
In the future it would be interesting to realize a sample in Kapton DuPont HN made entirely with an overlapping of layers and not with a partial overlap: in this way there would be no escape and the results would lead to a likely estimate.

Furthermore, an interesting measure was that with the second sample, constituted by three layers without overlap, at 142 K with helium as a permeating gas: the measurement was carried out twice, and in both times it reported only an accumulation of hydrogen and not helium. This is probably due to the fact that the sample in the previous measurements was so saturated with hydrogen, that it no longer had channels available in the lattice for helium, even after purging the channels after hydrogen measurements. This theory, if carried out, could reach interesting results, for applications in which helium is used as an operating gas and where the passage of hydrogen does not cause problems to the experiment.

Appendix A

Tab. A – Comparison of the hydrogen permeation results of all the three sample measured.

T [K]	1/T [1/K]	Pressure of injection [bar]	Kapton DuPont K [l/(m/s)]	Kapton Dupont HN 1, K [l/(m/s)]	Kapton Dupont HN 2, K [l/(m/s)]
179	0.005587	0.6	6.80E-12	2.95E-12	-
		0.8	6.61E-12	4.83E-12	-
		1	6.80E-12	5.10E-12	1.64E-12
197	0.005076	0.6	1.71E-11	5.99E-11	-
		0.8	1.96E-11	6.37E-11	-
		1	1.96E-11	6.47E-11	2.48E-12
226	0.004425	0.6	7.45E-11	3.79E-10	-
		0.8	7.55E-11	3.76E-10	-
		1	7.80E-11	5.25E-10	7.32E-12

Tab. B – Comparison between the helium permeation results (since for the third sample hydrogen at 1000 mbar has been injected, it is represented in a table a part, see Tab.C).

T [K]	1/T [1/K]	Pressure of injection [bar]	Kapton DuPont K [l/(m/s)]	Kapton Dupont HN 1, K [l/(m/s)]
142	0.007042	0.8	6.50E-13	-
179	0.005587	0.8	1.46E-11	1.59E-11
197	0.005076	0.8	5.60E-11	8.85E-11
226	0.004425	0.8	1.21E-10	1.49E-10
250	0.004	0.8	2.47E-10	5.27E-10

Tab. C – Permeation helium results for the third sample made by three layers in Kapton DuPont with an overlap.

T [K]	1/T [1/K]	Pressure of injection [bar]	Kapton DuPont HN2, K [l/(m*s)]
142	0.007042	1	3.09E-12
179	0.005587	1	5.87E-13
197	0.005076	1	1.86E-12
235	0.004255	1	2.02E-11

Tab. D – Comparison between the flux φ of injected gases obtained with the static and integrated methods, of all the samples.

Sample	Gas	Pressure of injection [bar]	T [K]	φstatic [(bar*l)/s]	φdynamic [(bar*l)/s]
1	H_2	0.6	179	4.43E-11	3.26E-12
1	H_2	0.8		3.79E-11	8.05E-13
1	H_2	1		5.11E-11	2.25E-11
1	H_2	0.6	197	7.71E-11	1.85E-10
1	H_2	0.8		1.18E-10	2.57E-10
1	H_2	1		1.47E-10	3.87E-10
1	H_2	0.6	226	3.36E-10	5.14E-10
1	H_2	0.8		4.54E-10	8.54E-08
1	H_2	1		5.85E-10	7.20E-10
1	He	0.8	142	3.90E-12	4.66E-11
1	He	0.8	179	8.75E-11	3.40E-11
1	He	0.8	197	3.36E-10	7.70E-12
1	He	0.8	226	7.24E-10	2.34E-13
1	He	0.8	250	9.20E-10	2.56E-13
2	H_2	0.6	179	1.33E-11	1.16E-12
2	H_2	0.8		2.90E-11	8.59E-12
2	H_2	1		3.83E-11	6.99E-11
2	H_2	0.6	197	2.70E-10	3.27E-11
2	H_2	0.8		4.04E-10	4.29E-11
2	H_2	1		4.86E-10	3.46E-10
2	H_2	0.6	226	1.71E-09	3.04E-11
2	H_2	0.8		2.25E-08	2.40E-10
2	H_2	1		1.85E-09	4.89E-10
2	He	0.8	142	-	-
2	He	0.8	179	9.51E-11	2.58E-12
2	He	0.8	197	5.31E-10	9.60E-12
2	He	0.8	226	8.94E-10	8.60E-10
2	He	0.8	250	3.16E-09	2.799E-11
2	He	0.8	142	-	-
3	H_2	1	179	1.38E-11	4.73E-13
3	H_2	1	197	2.09E-11	5.22E-12
3	H_2	1	226	6.15E-11	1.83E-12
3	He	1	142	2.60E-11	3.46E-12
3	He	1	179	4.93E-12	2.33E-12
3	He	1	197	1.56E-11	3.54E-12
3	He	1	235	1.69E-10	3.58E-11

Tab. E – Results of the activation energies of both hydrogen and helium for all the samples.

Gas	Kapton DuPont Ek [J/mol]	Kapton DuPont Ed [J/mol]	Kapton DuPont HN 1 Ek [J/mol]	Kapton DuPont HN 1 Ed [J/mol]	Kapton DuPont HN 2 Ek [J/mol]	Kapton DuPont HN 2 Ed [J/mol]
Hydrogen	1.69E+04	1.73E+04	3.08E+04	3.41E+04	1.10E+04	2.34E+04
Helium	1.64E+04	1.26E+04	1.67E+04	1.47E+04	4.57E+03	1.26E+04

Tab. F –Hydrogen permeation results at the COMPASS work temperature.

T [K]	1/T [1/K]	Kapton DuPont K [l/(m/s)]	Kapton Dupont HN 1, K [l/(m/s)]	Kapton Dupont HN 2, K [l/(m/s)]
20	0.05	3.88E-51	2.42E-83	4.34E-38

Tab. G –Results of diffusivity and solubility measurements of the three samples.

Sample	Gas	Pressure of injection [bar]	T [K]	D [(m^2)/s]	S [l/(m^3)]
1	H_2	0.6	179	1.07E-13	2.7E+01
1	H_2	0.8		3.26E-12	3.0E+01
1	H_2	1		3.17E-12	4.0E+01
1	H_2	0.6	197	3.47E-13	4.4E+01
1	H_2	0.8		3.26E-12	4.5E+01
1	H_2	1		1.69E-12	5.0E+01
1	H_2	0.6	226	1.63E-12	4.0E+01
1	H_2	0.8		2.50E-11	5.5E+01
1	H_2	1		3.40E-11	7.0E+01
1	He	0.8	142	2.30E-13	5.0E+00
1	He	0.8	179	1.63E-12	8.0E+00
1	He	0.8	197	1.63E-12	3.0E+01
1	He	0.8	226	2.24E-11	2.2E+02
1	He	0.8	250	1.62E-11	2.5E+02
2	H_2	0.6	179	5.20E-14	5.67+01
2	H_2	0.8		3.27E-13	1.48+01
2	H_2	1		5.94E-13	8.59+00
2	H_2	0.6	197	5.10E-13	1.17+02
2	H_2	0.8		4.36E-12	1.54E+02
2	H_2	1		2.41E-12	2.68E+02
2	H_2	0.6	226	6.22E-12	6.10+01
2	H_2	0.8		1.68E-10	2.23+01
2	H_2	1		3.92E-11	6.30+00
2	He	0.8	142	-	-
2	He	0.8	179	1.49E-12	8.50E+00

2	He	0.8	197	3.68E-12	8.12E+00
2	He	0.8	226	4.17E-12	2.85E+01
2	He	0.8	250	8.19E-12	2.19E+02
3	H_2	1	179	9.33E-15	1.79E+01
3	H_2	1	197	3.35E-13	7.42E+00
3	H_2	1	226	2.88E-13	2.84E+00
3	He	1	142	4.48E-11	7.74E+00
3	He	1	179	3.27E-10	2.01E+00
3	He	1	197	1.99E-09	1.05E+00
3	He	1	235	2.29E-09	9.88E-01

Bibliography

[1] wwwcompass.cern.ch/.

[2] Bremer J., Doshita N., Dufay L., Geyer R., Mallot G.K., Pirotte O., and Vullierme B., Liquid Hydrogen Target for the COMPASS experiment, 2014, Technical report n.1262259, CERN, 2014.

[3] Miyake H. et al., *J.Vac.Sci.Technol.A*, v.1(3), 1983.

[4] Laurenson L. e Dennis N.T.M., *J.Vac.Sci.Technol.A*, v.3(3), 1985.

[5] Bellachioma M.C., *Applicazione di film sottili per il controllo della diffusione e della permeabilita' di materiali polimerici per UHV*, CERN-THESIS-2004-060,2004.

[6] Baldanza A., *POLYMERIC CANDIDATES FOR COMPASS EXPERIMENT AT CERN: experimental techniques to measure gas permeability in polymers at extremely low temperatures*, CERN-THESIS-2016/2017.

[7] Da Silvia Sobrinho A.S. et al., Surf.Coat.Techn., v.116-119,1999.

[8] Da Silvia Sobrinho A.S. et al., J.Vac.Sci.Technol.A, v.18,2000.

[9] Bachmann S. et al., Nucl.instrum.Methods A., v.478, 2002.

[10] Bressan A. et al., Nucl.Instrum.Methods A, v.425, 1999.

[11] Bellachioma M.C. e Chuste G., *Outgassing Measurements of a GEM detector*, Technical Report n.34499, CERN, 2002.

[12] Mapes M. et al., J.Vac.Sci.Techn.A. v.12, 1994.

[13] Adams G., Rev.Sci.Instrum., v.511, 1997.

[14] Lafferty J.M., 1981, *Physics Today*.

[15] Benvenuti C. et al., 1998, J.Vac.Sci.Technol.A, v.16.

[16] *Understanting Vacuum and Vacuum Measurement*, Reál J. Fradette, Senior Technical Consultant, Solar Manifacturing, Inc.

[17] K. Jousten, *Gauges for fine and high vacuum*, Physikalisch-Technische Bundesanstalt, 10587 Berlin, Germany.

[18] K. Jousten, *Ultrahigh vacuum gauges*, Physikalisch-Technische Bundesanstalt, 10587 Berlin, Germany.

[19] K. Jousten, Vieweg Verlag, Wutz handbuch Vakuumtechnik.

[20] A. Roth, *Vacuum technology*, north-holland.

[21] Crank J., *The mathematics of Diffusion*, Oxford University Press, Washington, 1975.

[22] Kesting R. E., Fritzsche A. K., *Polymeric gas separation membranes*, John Wiley & Sons, Inc., New York, pp 862, 1987.

[23] Jessie A. Key, *Activation Energy and the Arrhenius Equation.*

[24] Stannett V., *The transport of gases in synthetic polymeric membranes – An historic perspective*, J. Membr. Sci., v.3, 1978.

[25] Crank J., *Methods of measurements in Diffusion in Polymers*, Academic Press, New York, pp1, 1968.

[26] Barrer R.M., *Diffusion in and through solids*, Cambridge University Press, London, 1951.

[27] Barrer R.M., *Diffusion in polymers*, Academic Press, New York, 1968.

[28] Barrer R.M., Phil. Mag., v.35, 1944.

[29] Barrer R.M., Porc.phys.Soc., v.58, 1946.

[30] V. Parma, *Cryostat Design*, CERN, Geneva, Switzerland.

[31] DuPont KAPTON®, POLYIMIDE FILM, general specifications, kapton.com.